ICFO – INSTITUTE OF PHOTONIC SCIENCES

UPC - BARCELONA TECH

Imaging cytometry technology for environmental and biomedical applications

JUAN MIGUEL PÉREZ ROSAS

Thesis advisor: Prof. Valerio Pruneri

PhD Thesis - 2020

A Inés y Juan Carlos.

Abstract

Early detection of microorganisms in environmental and biomedical applications is critical for the effective response to potential pathogenic treats. Most traditional methods and instrumentation for the analysis of these samples are becoming obsolete due to the fact that they are time-consuming and have long response times. Modern solutions are limited to high-end centralized facilities and specialized trained personnel, given their high-cost and complexity. There is thus a clear need to develop and introduce low-cost, easy to use, high-performance devices capable of rapidly identifying and quantifying pathogenic microorganisms in environmental and biomedical samples.

The work behind this thesis was devoted to the design, development and validation in relevant industrial environments of two image cytometry devices capable of characterizing biological and industrial samples in terms of their microorganism content. Bringing a potentially high-impact solution to the current industry need.

The first technology, defined within the context of this thesis as Fourier image cytometry, is an optical device capable of increasing the sample volume tested when compared to traditional state-of-the-art counterparts. By evaluating the sample in the Fourier domain, the device is capable of measuring characteristics of particulate within a sample volume larger than other imaging systems. The result is an enhancement of both field of view (FOV) and depth of field (DOF) of the target sample. Furthermore, the implementation of the Fourier image cytometer in this thesis is a portable and compact device comprising of low-cost optics and electronics. The design of the entire device was performed with the objective to minimize the cost and maximize the capabilities. This was possible mainly due to the recent advances in image sensor technologies that simplify the device's optics. In our Fourier imaging cytometry, LED light sources and conventional achromatic optical lenses are at the basis of device's optics as opposed to high-end lasers or optical microscopes. For the detection scheme, a CMOS image sensor was used.

After optimizing the prototype and going through rigorous validation in a laboratory, the Fourier image cytometry introduced in this thesis was validated in two relevant industrial environments. The device was tested using real environmental samples. In the first industrial validation, it was used for the microorganism's identification and quantification in water coming from cooling towers. The second industrial validation used a further optimized implementation of the cytometer to analyze fresh and marine waters for their microorganism population, specifically phytoplankton within the context of ballast water and ballast water treatment systems.

The second image cytometry designed, developed and implemented within the scope of this thesis, focused on detection of microorganisms spread over surfaces. Following the motivation for low-cost compact devices, a Surface cytometer was designed. The Surface cytometer is an optical device capable of quantifying bacterial population over a surface of over 300 mm^2. The device was completely autonomous thanks to the integration of a single-board computer within its design. The light source and detection scheme continued to be LED source and CMOS sensor detection. Similarly to the validation process of the Fourier cytometer, the Surface cytometer was tested in controlled samples in a laboratory environment, before it was put to test on a biomedical application for bacterial growth monitoring and compared to standard devices of measurement of optical density, used today in the industry.

In summary, in this thesis we present two novel image cytometers and three clear industrial applications in which the devices were validated. This clearly indicates the potential of image cytometry as an effective low cost and portable tool for the analysis of microorganisms in the environmental and biomedical sectors.

Resumen

La detección temprana de microorganismos en aplicaciones ambientales y biomédicas es crítica para la respuesta efectiva a posibles amenazas patogénicas. La mayoría de los métodos e instrumentos tradicionales para este tipo de análisis están casi obsoletas, debido a los esfuerzos que requieren y sus largos tiempos de respuesta. Las soluciones modernas se limitan a instalaciones centralizadas de alta gama y personal especializado, esto debido a su alto coste y complejidad. Existe una clara necesidad de desarrollar e introducir dispositivos de bajo costo, fáciles de usar y de alto rendimiento capaces de identificar y cuantificar rápidamente microorganismos patogénicos en muestras ambientales y biomédicas.

El trabajo detrás de esta tesis se dedicó al diseño, desarrollo y validación en entornos industriales relevantes de dos dispositivos de citometría de imagen capaces de caracterizar muestras biológicas e industriales en términos de su contenido de microorganismos. Aportando una solución con un potencial alto impacto a las necesidades actuales de la industria.

La primera tecnología, definida en el contexto de esta tesis como citometría de imagen de Fourier, es un dispositivo óptico capaz de aumentar el volumen de muestra capturado en comparación con las tecnologías tradicionales y el estado del arte. Al evaluar la muestra en el dominio de Fourier, el sistema es capaz de medir las características de las partículas dentro de un volumen de muestra mayor que los sistemas de imágenes comparativos. El sistema resultante mejora tanto el campo de visión (FOV, por sus siglas en inglés) como la profundidad de campo (DOF, por sus siglas en inglés) de la muestra. Además, la implementación del citómetro de imagen de Fourier en esta tesis es un dispositivo compacto y portátil compuesto por componentes ópticos y electrónicos de bajo coste. El diseño de todo el sistema se realizó con el objetivo de minimizar el coste del sistema y maximizar sus prestaciones. Esto fue posible principalmente debido a los recientes avances en las tecnologías de sensores de imagen que nos permitieron simplificar la óptica del dispositivo. En esta

implementación de la citometría de imagen de Fourier, fuentes de luz LED y las lentes ópticas acromáticas convencionales comprenden la óptica del sistema en lugar de láseres de alta gama u objetivos de microscopios ópticos. Para el esquema de detección se utilizó un sensor de imagen CMOS.

La citometría de imagen de Fourier presentada en esta tesis también fue validada en dos entornos industriales relevantes. Después de optimizar el prototipo y pasar por una validación rigurosa en un entorno de laboratorio. El sistema se probó utilizando muestras ambientales reales. En la primera validación industrial, el sistema se utilizó para la identificación y cuantificación del microorganismo en el agua proveniente de torres de refrigeración. La segunda validación industrial utilizó una implementación más optimizada del citómetro y se probó para analizar aguas dulces y marinas, y su población de microorganismos, específicamente la cuantificación de *phytoplankton* en el contexto de sistemas de tratamiento de aguas de lastre.

La segunda citometría de imagen diseñada, desarrollada e implementada dentro del alcance de esta tesis se centró en la detección de microorganismos sobre superficies. Siguiendo la motivación de los dispositivos compactos de bajo costo, se diseñó un citómetro de superficie. El citómetro de superficie es un dispositivo óptico capaz de cuantificar la población bacteriana en una superficie de más de 300 mm^2. El dispositivo es completamente autónomo gracias a la integración de una computadora de placa única dentro de su diseño. La fuente de luz y el esquema de detección continuaron siendo LED y sensor CMOS. De manera similar al proceso de validación del citómetro de Fourier, el citómetro de superficie se probó en muestras controladas en un entorno de laboratorio, antes de someterse a prueba en una aplicación biomédica para el monitoreo del crecimiento bacteriano y se comparó con los sistemas estándar de medición de densidad óptica, utilizados hoy en día. en la industria.

En resumen, en esta tesis presentamos dos nuevas tecnologías de citometría, junto con dos dispositivos de alto rendimiento (uno para cada tecnología) y tres aplicaciones industriales en las que las tecnologías fueron validadas. Esto demuestra el potencial de la citometría de imagen como una herramienta adecuada para el análisis de microorganismos en aplicaciones ambientales y biomédicas.

Acknowledgments

I have been debating myself on what the best approach to write these acknowledgements should be. My PhD has definitely been one of the toughest most relevant challenges in my life. A challenge that even though, I'm the sole author of this thesis, has involved the support of many others at a technical, social and emotional level. All of them have had an important role in this journey, all I can hope is this section will do them justice.

I must start of course with my parents Inés y Juan Carlos, to whom I dedicate this work. Their unconditional support has known no boundaries, my success is only thanks to their moral guidance and the education they've provided along with many other opportunities. Next to my parents I know I can always count with my sisters, Caro, Patry and Vero, being the youngest of 4 and the only boy had many privileges growing up, some that continue to cash in many years after. My sisters have always believed in me, perhaps more so than I do, that sense of pride they have in their "hermanito" is something very precious and valuable to me. The rest of my family has also played a role in this story, my grandparents are a clear example of succeeding under strenuous circumstances which has always been an incredible example and a core motivation to me. My aunts, uncles and cousins, I thank you all in many more ways than these words can hold.

Next to my family, I want to acknowledge my supervisor, Professor Valerio Pruneri. Valerio's guidance goes beyond the scope of this thesis, and don't get me wrong, he is owed much praise for the results herewith; but he had a much bigger impact in shaping my career. Valerio is an example of a visionary, of always having our minds set in the big picture and of not settling for less than we are able to achieve. Seeing Valerio lead such a diverse group and do so successfully has been inspirational to say the least. However, for the accomplishments throughout my PhD, focusing on the day to day and getting things done was instrumental in building the journey to that big picture, and for that I have Marc Jofre to thank, with Marc I learned many hard and soft skills that continue to be useful today. Many others played a role, I thank all of my co-authors and both internal and external collaborators that were with me through this journey.

Thinking beyond that professional support, being an expat from a big family is a very tough reality. Finding yourself alone in a foreign country can take its toll. Fortunately, alone is one thing I have never been. In Barcelona I have found so many people that have made this my home. Here's to my Family away from home and for the many beers we've had and the many more to come.

Annie, my longest constant. You've always been there to take my mind off work, and we both know that is a challenging thing. I thank you for everything you've given me, for taking me into your home, your family and your friends and making them my own.

Juancito, my brother from a whiter mother. Mi Pana, you know you truly are like a brother to me. I'm thankful that me leaving ICFO did not change this in the slightest. I'm honored to have been a witness to the loving relationship you and Sofi have built, and I'm thankful that through this Sofi has also grown to be a dear friend of mine.

To the Excelentísimo comité and its longest running members Miriam and Roland. My support system throughout my PhD, I cannot count the number of times I needed to vent, and you were there to listen. You've been there ever since you saw the "real" Juan on that first night in Apolo. I thank you and congratulate you, because this success is as much yours as it is mine, I know I would not have made it through without having you two there.

Mis cubanitos, Noslen y Alberto, we often found ourselves fighting over who's got the best rum and the worst dictator. I rather give you the dictator and take the rum, but by now it seems like a two-way tie. It's been great to have shared this journey with you.

To my drinking companions: Mike, Sarah, Silvana, Ferran, Pau and Lisa (not much of a drinker, but always energetic and fun). I treasure the friendship we have built over the years and I hope there are many more memorable moments in the horizon.

To the friends I have made on my later days at ICFO, or even after leaving: Dani (yes, we are friends and there's nothing you can do about it!), Ana, Sebas, Rubi and Manu. We have a short lived but certainly deep friendship that I hope continues to grow.

To Felix and Inge, your stay at ICFO was somewhat short but profound. I'm happy that our friendship has overcome geographical challenges and I look forward to seeing you succeed in your own journey soon.

To La Mamma (Vittoria), Waldo, Davide, Ilaria and Cesar. Thank you, because your experience helped me with technical challenges, but it was also a guiding light in navigating the intricacies of the academic life.

To Silvia and her team at KTT, namely Sergi and Sol with whom I shared the most, working in this area was one of the most interesting experiences of my PhD, which is easy to conclude given the steps I have taken afterwards.

To the ICONS team: Sandra, Pamina and Kavitha, I had a lot of fun strengthening this organization with you and I'm happy that we managed to bring IONS back home, albeit not soon enough for me to help.

Finally, to everyone else in the Opto family, past and present members, I'm very happy to have had a team of A-class colleagues.

Thank you!

List of Publications

Journal Papers

- J. M. Pérez, M. Jofre, P. Martínez, M. A. Yáñez, V. Catalan, V. Pruneri. “An image cytometer based on angular spatial frequency processing and its validation for rapid detection and quantification of waterborne microorganisms”. *Analyst* 140(22):7734-41, 2015.
- J. M. Pérez, M. Jofre, P. Martínez, M. A. Yáñez, V. Catalan, A. Parker, M. Veldhuis, V. Pruneri. “CMOS based image cytometry for detection of phytoplankton in ballast water”. *Biomedical Optics Express* Vol. 8 number 2, 1240, 2017.
- R. Sibilo*, J. M. Pérez*, F. Tebbenjohanns, C. Hurth, and V. Pruneri. “Surface cytometer for fluorescent detection and growth monitoring of bacteria over a large field-of-view”. Biomedical Optics Express Vol. 10 issue 4, 2101-2116 (2019). (*) equal contribution.

Patents

- J. M. Pérez, M. Jofre, V. Pruneri. “IMAGE CYTOMETER FOR CHARACTERIZATION AND QUANTIFICATION OF PARTICULATE SAMPLES”. US patent US10346972 (B2) also filed in Europe, China and Japan. Priority date 23/04/2015.
- J. M. Pérez, R. Sibilo, C. Hurth, V. Pruneri. “SURFACE CYTOMETRY FOR THE DETECTION OF FLUORESCENT PARTICLES”. PCT/ES2019/070058, filed in Europe. Priority date 07/02/2019.

Conference contributions

Talks

- J. M. Pérez, M. Jofre, P. Martínez, V. Pruneri. “Detection of Escherichia coli using image cytometry based on angular spatial frequency processing”. CLEO Europe 2015.
- J. M. Pérez, M. Jofre, P. Martínez, M. A. Yáñez, V. Catalan, A. Parker, M. VeldhuisV. Pruneri. “Fourier imaging cytometry for optical analysis of phytoplankton and bacteria in ballast water”. LAOP 2016.

Posters

- E. Soria, V. Catalán, M. A. Yáñez, M. A. Fernández, E. Hill, D. Trouchet, J. M. Pérez, H Bohlmann, S. González. “CYTO-WATER: An integrated and portable system for rapid response to Legionella and E. coli in environmental waters”. IWA 2016

Other relevant contributions

- M. Jofre, R.A. Terborg, A. Villar, P. Martínez, J.M. Pérez, D. Janner, I. Manneli, V. Pruneri. “The Next Generation CCD or CMOS Lens-free Microscopy for Bio-medical and Material Processing Analysis”. Advanced Photonics OSA 2014. Invited talk.
- M. Jofre, J.M. Pérez, R.A. Terborg, P. Martínez, J. Pello, V. Pruneri. “New designs of CMOS based lens-free microscopy for particles and cells analysis”. Blue Photonics – Optics in the Sea 2015. Invited talk.
- M. Jofre, J.M. Pérez, R.A. Terborg, P. Martínez, J. Pello, V. Pruneri. “Small form-factor lens-free microscopy for detection of particles, micro-organisms and proteins”. Micro Photonics 2015.
- M. Jofre, R.A. Terborg, J.M. Pérez, t. Coll, P. Martínez, W. Amaya, J. Pello, V. Pruneri. “Sensing of particles, micro-organisms and biomarkers using the camera of a mobile phone”. NanoBioMed 2016. Invited talk.

- M. Jofre, J M Perez, P Martinez, Z Mubarak, C Hurth, A Yañez, V Catalan, A Parker, M. Veldhuis, V Pruneri. “CMOS-based Image Cytometry for Detection of Phytoplankton in Ballast Water”. IMarEST Ballast Water Technology Conference 2017.

- J.M. Pérez, R.A. Terborg, T. Coll, P. Martínez, W. Amaya, C. Hurth, J. Pello, M. Jofre, V. Pruneri. “Large-field-of-view Cytometer and DIC Microscope using CMOS Image Sensor Arrays”. NyNa 2017. Invited talk.

- R.A. Terborg, J.M. Pérez, T. Coll, P. Martínez, W. Amaya, C. Hurth, J. Pello, M. Jofre, V. Pruneri. “CMOS-Based Cytometer and Differential Interference Contrast Sensing”. Imaging and Applied Optics 2017. Invited talk.

- J. M. Pérez, R.A. Terborg, T. Coll, P. Martínez, W. Amaya, C. Hurth, J. Pello, M. Jofre, V. Pruneri. “CMOS-based Cytometer for optical detection of marine microorganisms”. Photonics4Growth 2017.

Contents

List of Figures

List of Tables

1

Introduction

1.1. Overview of cytometry and image sensor devices for biosensing applications.

Cytometry is a process in which physical and/or chemical characteristics of single cells are measured[1]. The objectives are to analyze whether cells are present in the sample under analysis, how many cells there are and what kind of cells they are. The concept dates back to the late 19th century, when physiologists and anatomists started using blood cell counting chambers and optical microscopes to quantify blood cell concentration[2]. Over the 20th century, the reach and field of application of cytometry started to expand and now includes a variety of biological, clinical and technological applications in fields such as immunology, hematology, genetics and pathology.

Traditionally the most common examples of implementations in the field are flow cytometry and image cytometry, both of which are primarily optical techniques.

Flow cytometry is often used to analyze individual cells in a suspension and its key performance indicators are the analysis speed, detection sensitivity and the ability to measure two or more parameters simultaneously. Flow cytometers are based on the light-scattering properties of the cells being analyzed and their fluorescence emission. This fluorescence may be associated with dyes or conjugated to specific antibodies for molecules either on the surface or in the intracellular components of the cells. They were initially developed by immunologists for separating different cell populations, followed by coculture experiments to determine the function of cells within the immune system. This was achieved by using fluorescence activated cell sorting (FACS) on the flow cytometer. The initial instruments were able to analyze one or two colors of fluorescence but today, instruments capable of analyzing 11 colors of fluorescence are available[3]. Flow cytometry has proven to be a very effective technique when it comes to analyzing cells and their characteristics, which is perhaps why the flow cytometry market has been one of the fastest growing segments in life sciences[4]. However, one of the most significant applications of flow cytometry is clinical diagnosis, an area facing serious budgetary constraints in healthcare systems around the world[5]. The use of expensive technologies, devices or methods, like those required for flow cytometry, is not often justifiable for preclinical, outpatient care or biomedical laboratories. In most of these cases, the options are to either use obsolete methods or to outsource analysis to larger centralized facilities. Both options have a direct impact on the time taken to obtain results and the quality of such results. This is why the need for faster diagnostics through cost-efficient methods has motivated the advancement of the second vertical in the cytometry field, image cytometry.

Image cytometry is also used for the multiparameter analysis of cells but, as opposed to flow cytometry which analyses cells individually, a sample usually contains multiple adherent cells (high-content analysis)[6]. Sophisticated microscopes with laser sources, high-powered magnifying objectives and high sensitivity detectors are types of image cytometer, but in many ways, they share the cost restrains of flow cytometers. However, the advancement in image sensor technologies over the past decade has a great potential in substituting the expensive components (laser sources and high-power optics) of sophisticated microscopes with much cheaper options. These include light emitting diodes and lower cost optical equipment, which can be as little as half the price. In addition to the lower cost, image cytometers can be easily operated through direct cell imaging on a computer screen. For these two reasons (cost and ease of use), image cytometers are gradually entering into the market, as they offer a competitive alternative to flow cytometers in many applications.

1.2. **State of the art image cytometry and image sensor devices for biosensing applications.**

Given the potential shown in theory by novel image cytometry implementations, an effort has been made by the research community to advance optical technologies designed for the cytometry field and validate them in specific industrial applications and use cases. These novel techniques focus not only on creating cost-efficient versions of previous image cytometers but also, and perhaps more importantly, on advancing the field to improve the features and capabilities of these new devices and methods. These improvements are mainly driven by an interest in enhancing the system's sensitivity (smallest detectable concentration of cells) and resolution (smallest detectable cell size), given that these are the two main parameters measured in cytometry.

In order to enhance sensitivity, researches often augment the sample size analyzed. In an image cytometer this can be achieved in one of two ways, either by increasing the field of view (FOV), defined as the measured area of the sample under analysis, or by increasing the depth of field (DOF), defined as the measured depth of the sample under analysis. For further clarification, the area in the definition is measured on a plane perpendicular to the light source axis, whereas the depth is measured over said axis.

The following are some of the novel devices and techniques developed over the past few years to enhance FOV. A silo-filter CMOS for a chip-scale fluorescent microscope has been demonstrated reaching a spatial resolution of 10μm over a 6mmx4mm FOV [7]. A lens-less fluorescent microscope with a FOV of approximately 60mm^2 and spatial resolution of under 4μm has been designed using a fiber optic faceplate to conduct the fluorescence emission and a prism surface to reflect the excitation wavelength [8], [9]. A compact cell-phone attachment has been proven to work for dark-field imaging, using a lens-system that achieves a FOV of about 80mm^2 with a spatial resolution of 20μm [10]–[12].

Other novel devices and techniques have been developed over the past few years to enhance DOF. Micro-lens arrays have been used in this sense to build a single view-point microscope that results in an ultra-wide FOV [13]. They are also used as one of the key elements of Light Field Microscopy, which is a multi-viewpoint imaging technique that can be resolved by applying three-dimensional convolution algorithms to captured samples with a large DOF [14].

Nowadays, the applications for image cytometry go well beyond its blood cell count beginnings in the late 19th century. Today, systems that can rapidly process, identify and quantify cells and microorganisms are an important necessity in life sciences research, as well as in industrial applications in such areas as food processing and manufacturing, pharmaceutical drug discovery and trials, environmental monitoring, and clinical diagnostics. Particularly when it comes to microorganisms, it is a well-known fact that early detection is critical for both treatment and prevention of diseases, which is why it is vital to find alternatives that circumvent the use of time-consuming methods. Additionally, more value would be added if these techniques could be delivered in a cost-efficient solution that also minimizes the need for device-specific training.

1.3. Environmental monitoring and the EU CYTOWATER project.

Environmental monitoring of industrial waters, bathing waters and ballast water, among others is a relevant social issue. The early detection of *Legionella pneumophila (L. pneumophila)* and *Escherichia coli (E. coli)* in environmental waters is an important public health issue. In industrial waters, *L. pneumophila)* represents a dangerous health risk caused by the inhalation of bioaerosols coming from the bacteria. Industrial environments with cooling towers, evaporative condensers and air conditioning systems have been associated with high risks of Legionnaires' disease, the atypical pneumonia caused by *L. pneumophila*. *E. coli*, on the other hand, is commonly used as a fecal pollution index and monitor in bathing waters in order to control the presence of waterborne pathogens.

The objective of the European project CYTOWATER (http://www.cytowater.eu/) was to create a new system for the detection and quantification of microorganisms in industrial and environmental waters. The resulting system was to be the integrated result of three main sub-systems: a water concentrating system for sampling, a microfluidics system for sample processing and an image cytometer for the identification and quantification of the pathogens of interest. The validation of the image cytometer in an industrial setup was an essential step for the overall system.

1.4. Aim of the thesis.

The main aim of this thesis is the design and development of novel image cytometers and their subsequent validation in relevant industrial application environments. Specifically, two image cytometers were designed, developed and validated, both of which have advanced the field in their own distinctive ways. The first image cytometer introduced the concept of Fourier image cytometry, and was validated in environmental monitoring applications which includes, but it is not limited to, those within the scope of the CYTOWATER project. The second image cytometer furthered the concept of surface cytometry and was validated for bacterial growth monitoring within the laboratory environment. Specific objectives of the thesis include:

- Development and adaptation of the image cytometers and the necessary computational algorithms for sample acquisition and processing to identify and quantify microorganisms.
- Validation of the Fourier image cytometer in two key industrial environments: cooling towers and ballast water.

1.5. Thesis outline.

The thesis contains the following chapters:

Chapter 2

Starting from the overview and introduction to cytometry, and the evolution of the field to its current state of the art, the Fourier image cytometry concept is introduced. Additionally, the chapter goes on to explain in detailed the design of the device in its preferred embodiment and reviews the proof of concept early results.

Chapter 3

Introduces in more detail the background and challenges surrounding the industrial and environmental applications, in which the newly introduced Fourier image cytometer was initially validated. The chapter goes on to explain the specific experimental realization of said validation and reviews the results including those of samples from cooling towers.

Chapter 4

Introduces a second industrial application in which the Fourier image cytometer was validated. Goes in detail as to the relevance of ballast water monitoring and treatment systems, describes the experimental realization and reviews the results obtained from the variety of systems and samples tested.

Chapter 5

Moves on to introduce the second image cytometer designed and developed within the scope of this thesis. The chapter introduces some background on the challenges of surface detection and some of the novel techniques approached for such objective. The design and implementation of the surface cytometer is described along with the experimental realization for its validation and a review of the results in microbiological growth monitoring.

2

Fourier imaging cytometry

2.1. Introduction. Applications and challenges.

Optical technologies can be very powerful when it comes to detecting minute quantities of particulate in industrial, biological and pathogenic samples. In chapter 1 we reviewed some of the more traditional and standardized solutions readily available on the market, which, in one way or another, make use of optical technologies for particulate analysis. These solutions share a few key disadvantages in that they are bulky and expensive due to their cumbersome assembly and the high cost of the optical components forming them. We then went on to review the results of the technological advances in optics and photonics research that have led us to more modern, compact and cost-efficient imaging solutions, some of which are also inexpensive in general. These solutions have come in particular from breakthrough developments in low-cost imaging technologies such as charged-coupled-devices (CCD) and complementary-metal-oxide-semiconductors (CMOS). The great potential and growing use of CCDs and CMOS sensors in image sensing devices has had an impact on cost reduction of up to two orders of magnitude. The main reason behind these cost savings is that the use of CCD and CMOS as detectors allows us to replace expensive laser source light emitting diodes (LEDs) and sophisticated microscopes with simpler proximity detection schemes.

In this chapter, we will introduce an innovative optical system for the analysis of particulate samples and the basic principles behind its operation, as well as the detailed design and implementation of such a device. Chapters 3 and 4 of this thesis will elaborate on the use of this device in industrial applications.

2.2. Background. Computational imaging and light field microscopy.

The design of our innovative system started with the analysis of the strengths and limitations of state-of-the-art image sensing solutions for particulate analysis. This directed the efforts to two key emerging trends, computational imaging, which focuses on simplifying the devices in size and complexity, and light field microscopy, which focuses on enhancing traditional systems through a clever adaptation of their optomechanics.

Computational imaging has the benefit of significantly lowering the size of the optical devices and the use of sophisticated optics for detection. By simplifying the optics, these systems inherently gain more field of view (FOV). Be it by using imaging lenses of weaker focus or by eliminating the lenses altogether, these implementations can enhance the FOV to at least the size of their detector. The drawback, however, is that the oversimplification of the optomechanics comes at a high computational cost. The absence of a strong focusing objective means that in order to recover information on the particulates within the measured samples, images must be processed with complex bespoke algorithms to recover the sample information and recreate an in-focus image.

Light field microscopy is a technique capable of capturing light fields of particulate samples. This is achieved by inserting a microlens array into the optical path of a conventional microscope. To compensate for the diffraction effects, a focus stacking imaging technique is applied to recover the sample’s light field. Focus stacking results from taking multiple captures at different focal distances, creating an image with a greater depth of field (DOF). With this technique, multiple reconstructions of the captured image can be retrieved. This is because, by using the microlens array, the detected full sample is composed of several sub-images, one for every microlens. By taking one pixel from each sub-image, different perspectives of the captured sample can be recovered, thereby giving an increased DOF.

2.3. Principles of Fourier imaging cytometry.

We have designed and implemented an optical system capable of analyzing particulate samples with an enhanced FOV and DOF, thereby creating a system that takes the combined strengths of these state-of-the-art features and overcomes their individual differences. The aim was to build a system that continued to be comprised of relatively inexpensive components but at the same time minimizing the computational cost of recovering data from the measurements.

Both state-of-the-art methodologies detect the particulate samples in the space domain (Real domain). The space domain implies a tradeoff between spatial resolution, FOV and DOF. For instance, in light field microscopy, an enhanced DOF is achieved by maintaining a fixed FOV (the same as for an unmodified microscope) but sacrificing spatial resolution. Computational imaging also increases the FOV by sacrificing spatial resolution but without any improvement in the DOF. By using complex reconstruction algorithms, the spatial resolution of computational imaging systems can be increased to below pixel size, but nothing is gained on the DOF.

The principle behind our innovative device is the far-field detection of the light field that interacts with the particulate sample. This means detecting and analyzing the sample in the spatial frequency domain (Fourier domain) instead of the Real domain, thereby improving, to the extent permitted by our optics, the trade-off between spatial resolution, FOV and DOF.

2.4. Device design based on Fourier optics principles.

The first step in our configuration is to enable the far-field detection in an economic proximity detection scheme, by performing the optical Fourier transform of an incoming light field. The information to be Fourier transformed is introduced into the system by a sample with an amplitude that is proportional to the input function of interest.

The concept is to design an apparatus capable of performing such a transformation and detecting the signal in it by means of an image sensor. With the intention of simplifying the post-processing of the captured signal and further increasing the DOF of the optical system, the Fourier transformed signal will be physically sampled by a spatially selective filter. This will in turn generate a set of sub-images on our detection plane, each of which contains amplitude and frequency information on our initial sample.

Specifically, the apparatus works as follows. The sample is illuminated by a wavelength limited light source, the interaction between the sample and the light source resulting in a broad band of spatial frequencies. This emission is an incoherent process; thus, the intensities sum up and do not give rise to interference effects. The sample is placed in front of an optical transforming element, an example of which is a converging lens. Another example of an optical component with such transforming properties is a curved mirror. A curved mirror can act as a converging lens, given a radius curvature equal to twice the focal length of said lens.

Finally, we position the spatially selective filter at the Fourier plane of our optical system to create the sub-images that are consequently captured by the image sensor positioned in proximity to the filter.

An optical converging lens was used as a transforming element for the specific design that we will review in this chapter and that was subsequently validated in an industrial application described in chapter 3. Such a lens inherently performs a two-dimensional Fourier transform, as will be explained.

Consider the general geometry where a sample, located in front of the lens, is

illuminated by a normally incident plane wave of amplitude A. Amplitude transmittance of the sample is represented by t_A. In this case, the beam leaving the sample and incident on the lens can be described with equation 2.1.

$$U_L(x,y) = A \cdot t_A(x,y) \tag{2.1}$$

The effects of the lens on the incident optical beam due to the optics can be described with equation 2.2.

$$t_l(x,y) = exp \cdot \left[-j \cdot \frac{k}{2 \cdot f} \cdot (x^2 + y^2)\right] \tag{2.2}$$

The amplitude distribution behind the lens becomes:

$$U'_L(x,y) = U_L(x,y) \cdot exp \cdot \left[-j \cdot \frac{k}{2 \cdot f} \cdot (x^2 - y^2)\right] \tag{2.3}$$

Using the Fresnel diffraction formula, one can find the distribution $U_f(u,v)$ at a distance z from the lens:

$$
\begin{aligned}
U_f(u,v) = \Big\{ & exp \cdot \left[j \cdot \frac{k}{2 \cdot z} \cdot (u^2 + v^2) \right] \cdot \frac{1}{j \cdot \lambda \cdot z} \\
& \cdot \iint U_L(x,y) \cdot exp \cdot \left[-j \cdot \frac{k}{2 \cdot z} \cdot (x^2 + y^2) \right] \\
& \cdot exp \cdot \left[j \cdot \frac{k}{2 \cdot z} \cdot (x^2 + y^2) \right] \cdot exp \\
& \cdot \left[-j \cdot \frac{2 \cdot \pi}{\lambda \cdot z} \cdot (x \cdot u + y \cdot v) \right] dxdy \Big\}
\end{aligned} \tag{2.4}
$$

The distribution $U_f(u,v)$ in equation 2.4 is the light field U'_L of equation 2.3 propagated to a distance z. From this we can conclude that the field distribution $U_f(u,v)$ is proportional to the two-dimensional Fourier transform of the incident field subtended by the lens aperture.

Finally, the Fourier transform of the beam after the sample volume is imaged at a distance f after the converging lens ($z = f$), meaning our image sensor is placed a distance f from the lens. The complex amplitude distribution of the field in the focal plane of the lens ($U_f(u,v)$) is the Fraunhofer diffraction pattern of the field incident on the lens ($U_L(x,y)$). The amplitude and phase of the light at coordinates *u and v* are related to the amplitude and phase of the input spectrum at frequencies $u/\lambda f$ and $v/\lambda f$, respectively, where f is the focal length of the converging lens and λ the incident wavelength.

The Fourier transform relation between the amplitude of the input light field ($U_L(x,y)$) and the amplitude of the light field at the focal-plane ($U_f(u,v)$) is not a complete one, due to the presence of the quadratic phase factor that precedes the integral in equation 2.4, while the phase distribution of $U_L(x,y)$ is not the same as the phase distribution of $U_f(u,v)$. The difference between the two is a simple phase curvature. In the case of the proposed design, where ultimately the signal would be captured by an image sensor, only the intensity of $U_f(u,v)$ is of real interest. Our detector cannot record phase information, and for this reason, phase curvature can be dismissed. This phase term is important if the goal is to calculate another field distribution after further propagation, in which case the complete complex field is needed. In our case, however, the intensity distribution in the focal plane will be recorded and the phase distribution is of no consequence. Measurement of the intensity distribution yields knowledge of the power spectrum of the input and, from this spectrum, it is possible to retrieve information linked to the nature of the sample.

That said, the input sample is located at a distance *d* from the lens and can vary between *f* (the focal length of the lens) and approximately zero (directly against the lens). If an exact Fourier transform relation to the sample is of prime interest, it is preferable to place the sample directly against the lens to minimize vignetting. However, for our measure of intensity it is convenient to place the sample at a distance equal to the focal length, where the transform relation is unencumbered by quadratic phase errors.

In conclusion, in the conceptual design of our apparatus, a collimated bandlimited light source will illuminate a sample positioned at a distance equal to the focal length of a converging lens used as a transforming element. At the output side of the lens and at a distance equal to its focal length, an image sensor detector will capture the light field.

Just before the image sensor, our light field is physically sampled by means of a spatial filter. In our specific implementation we have used a microlens array for this purpose. However, examples of this spatially selective filter can be any two-dimensional array-like structure built of several apertures capable of spatially filtering an incoming light field. Each aperture, in our case each microlens, selects a portion of the incoming light field preserving information about both its amplitude and phase.

The pitch of the lens array, or any other structure complying with the specifications, will define the periodicity of the sub-images captured by the image sensor, while the aperture of the microlenses, will define the spatial filtering capabilities.

In the case of a microlens array configuration, filtering capabilities are defined by the angular aperture of each microlens (N_m) as shown in equation 2.5.

$$N_m = \frac{f_m}{D_m} \tag{2.5}$$

In this equation, f_m represents the focal length of each microlens and D_m its diameter.

The microlens array works as an array of point scanning microscope objectives over the optical Fourier transform of the sample.

The image sensor capturing the signal filtered by the microlens array can be of several different technologies such as CCDs or CMOS sensors.

Once the light field is captured by our apparatus, the following processes are all digital and consist of the signal processing and data extraction from the collected sub-images.

This data extraction follows the principles of Fourier optics and the detected pattern intensity is given by equation 2.6.

In the case of two-dimensional geometry, this represents spatial frequency distribution. The center of the image is zero spatial frequency and each of the other intensity points $(n\lambda Z_i f_0)$ represents a harmonic of the captured signal.

Each of the sub-images contains aggregated information on several of these harmonics (spatial frequency information). By analyzing the spatial frequency information and the captured intensity, one can arrive at a statistical calculation of particulate count and size in the interrogated volume.

2.5. Fourier imaging cytometry device implementation.

In this section, we will review the initial implementation of the Fourier imaging cytometer (I-CYT). The I-CYT is an optical device whose design is based on the principles of Fourier optics and the mission to overcome FOV and DOF limitations in alternative technologies. Figure 2.1 is a photograph of two early laboratory implementations of the alpha prototype, corresponding to two different optomechanical assemblies. Both implementations used an achromatic optical lens of 30mm focal length as an optical transforming element and a microlens array of 10mmx10mm with a 300μm pitch and 18mm focal length. The difference between the implementations was the light source used. On the left side of the image, we see a prototype built with a free space LED which was controlled with an aperture and collimated with a combination of two achromatic lenses of 30mm and 50mm focal length. The collimated beam traversed the sample at approximately 30mm from the optical lens. On the right side of the image we see a prototype built with a fiber optic coupled LED. This was a multimode fiber coupled to a bandlimited LED. To further collimate the beam, the same combination of lenses was used as in the free space version.

Figure 2.1: Photo of two early laboratory implementations. This was an alpha prototype in which two different optomechanical assemblies were built. Both implementations used an achromatic optical lens of 30mm focal length as an optical transforming element and microlens arrays of 10mmx10mm with a 300µm pitch and 18mm focal length. The difference between implementations was in the light source used. On the left side of the image we see a prototype built with a free space LED. On the right side of the image we see a prototype built with a fiber optic coupled LED.

Both prototypes shared controlling electronics and power supplies. The LEDs were driven by a pulse width modulation (PWM) current source of up to 1A. The current source was operated by our customized software via a USB connection. Our software was capable of independently driving up to 6 light sources (only two of which were used in this prototype) with a minimum period of 50ns. The image sensors used were color CMOS sensors of 5MP with a 2.2µm pixel size and a Bayer filter configuration. The image sensor signal was also controlled with our customized software via USB. Our software was able to independently capture all four channels of the sensor (given the Bayer filter configuration), i.e., two green, one blue and one red channel. Each channel was analyzed independently and at times used for compensation. Images could be captured in low dynamic range (LDR) or high dynamic range (HDR) using our own implementations of standard algorithms. For the LDR we performed an optimization of exposure time and gains and then performed multiple captures with fixed parameters, which were then averaged before processing. For the HDR an initial and final exposure time could be set and a sweeping of these was performed at fixed gains, all of which were ultimately averaged using a weighting algorithm.

We performed minimum testing of these protypes with fluorescent and non-fluorescent polystyrene beads of multiple sizes but quickly moved on to their validation in industrially relevant applications and samples as we will demonstrate in the following chapters.

2.6. Conclusions.

In this chapter, we started with an introduction to the cytometry applications and the different limitations of current standards and emerging technologies. We then went on to establish the principles of our Fourier imaging cytometry, stating our intention to design and implement an optical device with enhanced FOV and DOF while maintaining a generally low-cost and simple opto-mechanical assembly. This led us to an in-depth study of the principles behind Fourier optics and how they could be applied to our advantage, which subsequently allowed us to design the conceptual approach of our apparatus. Finally, we went on to implement this design in a laboratory prototype whose industrialization and validation in relevant environments will be the focus of the following two chapters.

3

Industrial and environmental applications of Fourier imaging cytometry

The information, text and figures in this chapter have been adapted, under the terms of the Creative Commons Attribution Non-commercial license, from the original publication: "An image cytometer based on angular spatial frequency processing and its validation for rapid detection and quantification of waterborne microorganisms", J. M. Pérez, M. Jofre, P. Martinez, M. A Yáñez, V. Catalan, V. Pruneri. Analyst, 2015, 140, 7734-7741.

3.1. Introduction. Application-specific challenges.

In this chapter, we introduce how the newly designed I-CYT presented in chapter 2 can be applied for rapid detection and quantification of waterborne microorganisms. The I-CYT described herein is composed of off-the-shelf components and can analyze particulates within a sample volume of up to 350 µl, in a single snapshot.

In all imaging systems, a sample is illuminated by an incident light beam. After the sample, an optical lens can be placed to form the image plane and, inherently, the Fourier plane. For classical imaging systems, the detector is placed at the image plane, which corresponds to the plane where a replica of the sample (an image) is created and can in turn be captured by placing a detector at this plane. However, as discussed in chapter 2, in the proposed I-CYT the detector is placed at the Fourier plane, which corresponds to the plane where the optical Fourier transform of the sample is created. In this configuration, the detected image corresponds to the Fourier transform (FT) of our sample in the spatial frequency domain (*Figure 3.1*). Furthermore, the transmitted beam is spatially filtered in a set of sub-images by using a microlens array (MLA) just before being detected by a CMOS image sensor, resulting in an increased FOV and DOF.

Note that imaging systems that analyze the data in the Fourier domain have already been reported[15]–[17]. However, the newly designed I-CYT makes it possible to retrieve the sample information without the need for lengthy and complex digital transformations of high computational cost.

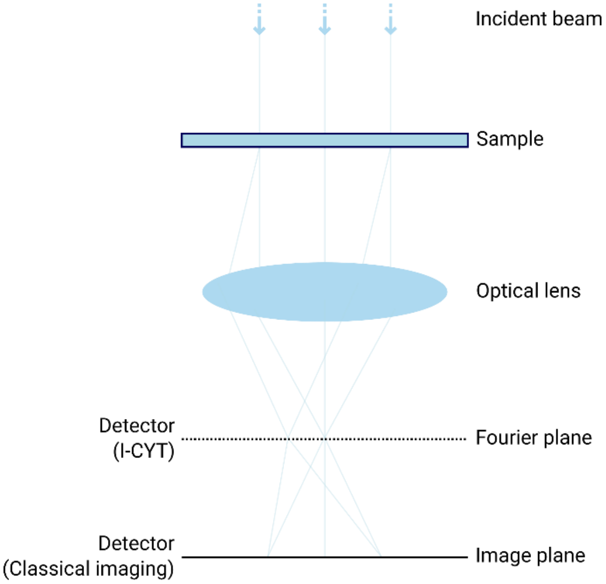

Figure ***Error! No text of specified style in document.****3.2: Comparison between classical imaging and the I-CYT; the location of the detector in each scheme is indicated.*

The focus on the analysis of waterborne microorganisms is driven by the importance of early detection of pathogenic sub-groups and their critical role for effective treatment and disease prevention. In many cases, diagnosis requires time-consuming, costly procedures and instruments, thus limiting their use to centralized settings with relatively advanced infrastructures and well-trained healthcare professionals[10]. Waterborne diseases cost the healthcare system in the United States over US$ 500 million per annum, with a similar amount reported in Europe; investments in early detection could lead to prevention of diseases and significant healthcare cost savings [18]. In both developing and industrialized nations, a growing number of contaminants from human activities are entering water supplies[19]. Parasitic infections and diarrheal diseases caused by waterborne bacteria have become a leading cause of malnutrition due to poor digestion of the food eaten by people made sick by the water [20]. In recent years, for example, the pathogenic role of *Escherichia coli* (*E. coli*) has increased, as it can cause a variety of infections in humans. *E. coli* is the most frequent cause of bloodstream infections and urinary tract infections, causes neonatal meningitis and is responsible for many foodborne infections worldwide [21].

Over the past few years, imaging systems have increasingly used CMOS or CCD image sensors to capture cells located on a microscope slide or in a transparent chamber and analyze thousands of them at once. For example, a chip-scale fluorescent system has been demonstrated, reaching a spatial resolution of 10 µm over a FOV of 24 mm^2 [22]. A more complex lensless fluorescent system with a FOV of 60 mm^2 and spatial resolution below 4 µm has been designed using a fiber optic faceplate[8], [9]. A 3D printed accessory has also been applied to a cell-phone for fluorescence imaging [11], [12], [23]–[25]. Besides resolution and FOV, the DOF is another important parameter to quantify the capability of a microscopy system, as it has a direct impact on the volume the system can analyze. Microlens arrays (MLAs) have been used to increase DOF by multi-view point imaging [14] and for fluorescence quantification [26].

In this study, we validate the I-CYT through the detection of the following waterborne microorganisms: *Escherichia coli* (*E. coli*), *Legionella pneumophila* (*L. pneumophila), Saccharomyces cerevisiae (S. cerevisiae)* and a saltwater diatom (phytoplankton). *E. coli* and *S. cerevisiae* are the most widely studied prokaryotic and eukaryotic model organisms, respectively [27]. Furthermore, *S. cerevisiae* is a type of yeast used extensively in food production [28] and, therefore, its detection and control have significant industrial interest. *L. pneumophila* is one of the main causes of severe atypical pneumonias in humans and it is present in soil, and natural and man-made aquatic environments [29]. Finally, phytoplankton microorganisms play a significant role in ballast water contamination, as we will explore extensively in chapter 4.

3.2. Experimental realization.

Design of the image cytometer (I-CYT)

The I-CYT was designed following the specifications detailed in chapter 2, in which an incoherent light source illuminates a sample and the beam resulting from the interaction with the sample is collected by an optical lens. At the Fourier plane, the beam is sampled by an MLA and detected by a CMOS image sensor.

Data extraction is based on Fourier optics principles. The center of the detected pattern is the zero spatial frequency component while the n-th order harmonic component is located at a distance $n \cdot \lambda \cdot Z_i \cdot f_0$ from the center, where λ is the wavelength, Z_i is the distance from the lens to the MLA (distance to the Fourier plane) and f_0 is the lens's focal length. From the statistical analysis of the captured sub-images, one can determine essential parameters, such as an estimation of particulate size in the original sample, particulate count (quantification) and particulate absorption, the latter as a measure of particulate complexity. The size and complexity distributions can be used to achieve specificity and differentiate particle populations. The count can be used to estimate the concentration of particles in a given sample.

To further increase the specificity of the system, fluorescence labelling of particles can be used. This requires that a specific excitation wavelength be selected, with a suitable set of filters placed before and after the sample. For the results presented in this chapter, fluorescein isothiocyanate (FITC) has been used as a fluorescent dye. FITC has excitation and emission spectra centered at 495 nm and 519 nm, respectively. In the case of the label-free results presented, a set of two polarizers replace the fluorescent filters to increase the sensitivity of the system. The polarizers are configured at a ninety-degree shift from one another to suppress the original light source and only detect the changes in our optical system introduced by the sample.

Figure 3.2 shows the schematic of the I-CYT system and a photo of the laboratory prototype (excluding controlling electronics). The system is comprised of: a red, green and blue (RGB) fiber coupled LED light source emitting at wavelengths 465 nm, 515 nm and 635 nm, respectively, an optical lens with a focal length of 30 mm, an MLA with an area of 10×10 mm^2 and a pitch of 300 µm, and two ultrahigh contrast linear polarizers with a maximum cross polarized transmission of 0.02%, 0.018% and 0.015% at 450, 550 and 650 nm, respectively; finally, a 5 Mega pixel (MP) CMOS color image sensor with 2.2 µm pixel size is used for detection. The CMOS sensor is equipped with a Bayer filter (RGB array of pixels) to enable color detection. A quartz flow cell is used to contain the sample. By placing the sample in close proximity to the optical lens, which results in a magnification factor of approximately one, the system can achieve a FOV of over 24 mm^2 (the complete area of the CMOS sensor). The MLA is placed at a distance from the lens equal to its focal length, in order to discretize the optical Fourier transform in sub-images, detected in specific regions of the CMOS placed in proximity to the MLA. By using the MLA as a multi-aperture optical part to spatially filter the frequency information of the sample, the resulting DOF is significantly increased in comparison to classical imaging systems from a few µm to what we estimate to be approximately 1 mm. When FITC labelling is used, the light source is substituted by a free space LED with the emission centered at 470 nm, followed by a pump filter centered at 466 nm, with a 40 nm bandwidth and 60 dB extinction ratio, and a fluorescent filter centered at 520 nm, with 36 nm bandwidth and 60 dB extinction ratio. The linear polarizers are replaced by the set of filters in this configuration.

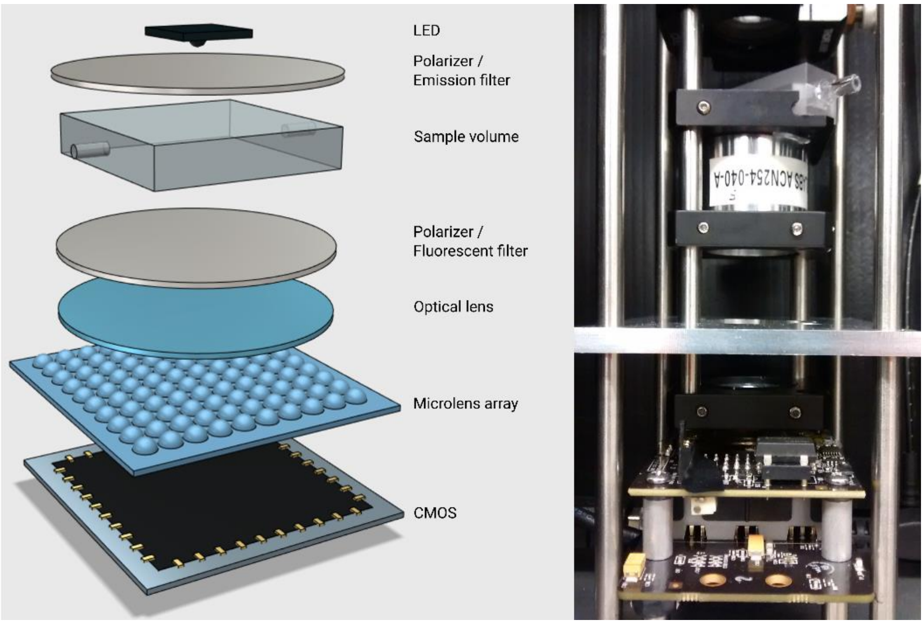

Figure 3.3: Schematic of the I-CYT system and a photo of the laboratory prototype (excluding controlling electronics). It is composed of a light source, a flow cell chamber that contains the sample volume, an optical lens, a microlens array and a CMOS sensor. Two polarizers or fluorescent filters (depending on the configuration) are placed before and after the sample volume. The distance between the light source and the CMOS sensor is about 95 mm.

The information processing capacity of an imaging system and its sensitivity (smallest differentiable feature) can be analyzed in terms of the spatial bandwidth product (SBP). Fourier holograms and their influence on the SBP have been extensively studied; the required SBP for a detector to ensure no loss of sample information is given by equations (1) and (2)[30].

$$SBP = \lambda \cdot d_1 \cdot 2 \cdot {v_{max}}^2 \tag{3.1}$$

$$SBP = \lambda \cdot d_1 \cdot 2 \cdot \left(\frac{1}{\delta_{min}}\right)^2 \tag{3.2}$$

As shown, the SBP of a Fourier hologram depends on the wavelength (λ), the distance of the sample from the detector (d_1) and the maximum recorded spatial frequency (v_{max}) or its inverse value, which is the minimum resolvable feature (δ_{min}). However, equations (1) and (2) are only valid under the assumption of an ideal lens with infinite aperture as a transforming element. The designed I-CYT comprises an optical lens of finite aperture which results in the attenuation of high spatial frequency components, known as the vignetting effect [31]. Equations (3)-(5) below describe this vignetting effect, in which the attenuation of the spatial frequencies (v) depends on the size of the illuminated sample (A), the dimension of the optical lens (D_L) and the distance between the sample and the optical lens (d_2). Equation (3) describes the conditions for the absence of spectral attenuation, equation (4), partial attenuation and equation (5), complete attenuation.

$$|v| < \frac{D_L - A}{2 \cdot \lambda \cdot d_2} \tag{3.3}$$

$$\frac{D_L - A}{2 \cdot \lambda \cdot d_2} < |v| < \frac{D_L + A}{2 \cdot \lambda \cdot d_2} \tag{3.4}$$

$$|v| < \frac{D_L + A}{2 \cdot \lambda \cdot d_2} \tag{3.5}$$

With the described system specifications and the mathematical modeling of equations (3)-(5), one can infer that the proposed I-CYT has (in theory) the capacity to detect and acquire information of particles as small as 0.98 µm, with partial spatial frequency attenuation below 5 µm.

The CMOS image sensor of the laboratory prototype had a dimension of 5.70 mm × 4.28 mm, which, combined with the MLA, allowed for the detection of 221 sub-images containing spatial frequency information of the captured sample. From each sub-image, the particulate size, complexity and count are computed. The distance between the MLA and the CMOS sensor is carefully adjusted on the Z axis so as to create non-overlapping sub-images (avoiding aliasing) without resorting to sub-sampling (information loss). The optimum Z location of the MLA for this configuration of the I-CYT is at the microlens focal length.

The LED source is collimated using an achromatic lens and a graduated iris diaphragm. The collimation of the light source is of special importance as it enables uniform illumination and it also improves performance of optical filters and linear polarizers. However, in practice, the sample is illuminated with a Gaussian wavefront; this implies an even lower signal to noise ratio for high spatial frequencies, in addition to the vignetting effects previously mentioned.

For the experiments reported in this chapter, we applied the signal processing methodology discussed below, in order to partially counteract this effect.

After capturing the sample volume image, the first processing steps are normalization and noise removal, which are accomplished by using a reference capture and a dark noise capture, respectively. The reference capture is the image with no sample in place, while the dark noise capture is the image with the light source turned completely off to account for the different noisy effects of the CMOS sensor. Next, the interrogated sample is deconvoluted with a control sample for compensation. The control is a sample with zero particulate and preferably in the same buffer solution or medium as that of the interrogated sample. Once the deconvolution is performed, the recovered sample is divided into the 221 sub-images and processed to retrieve the complexity, size and count information.

The complexity parameter is taken as a measure of particulate absorption. It is calculated by analyzing the contrast of the sub-image. The sub-image maximum intensity (I_{max}) is contrasted against the mean value of the lowest 1% luminance of the complete image (the composition of all 221 sub-images). The size information is calculated by analyzing the patterns in each sub-image. A main lobe region is detected, and its area is measured. The main lobe corresponds to the largest pattern within the sub-image, with the area measured at the 3 dB point (where the intensity of the lobe is at half maximum). Finally, the counting of the particulates is achieved by integrating and averaging the pixel intensities of each sub-image. For label-free detection, the presence of particulates within the sample volume results in the scattering of the incoming beam, which is detected by the image sensor. For the fluorescence detection, the target microorganism is excited and emits at the corresponding fluorescence wavelength captured by the CMOS image sensor. These pixel intensities from either scattering or fluorescence emission have a linear response, after the analog to digital conversion of the CMOS sensor's response. The linear measurements can be transformed into a logarithmic scale to provide results as an estimated count of cells per ml; this is done after calibrating the system with a known serial dilution.

Sample preparation

In order to validate the performance of the I-CYT with waterborne microorganisms, a set of samples of *Escherichia coli* (*E.* coli), *Legionella pneumophila* (*L. pneumophila), Saccharomyces cerevisiae (S. cerevisiae)* and a saltwater diatom (phytoplankton) were prepared. The *S. cerevisiae* and phytoplankton organisms were purchased as fresh cultures. The *L. pneumophila* and *E. coli* microorganisms were grown in the laboratory. The *L. pneumophila* was incubated for 3 days at 37 °C in a 5% CO_2 atmosphere on a Buffered Charcoal Yeast extract medium (BCYE). The *E. coli* was incubated for 24 hours at 37 °C on Tergitol-7 agar. The cells were harvested, and 10-fold serially diluted suspensions in Phosphate Buffered Saline (PBS) were prepared.

A second serial 10-fold dilution of *E. coli* was prepared, but in this case, using water from a cooling tower as a diluent, and the samples were treated with an anti-*E. coli* O + *E. coli* K (FITC) antibody by Abcam for fluorescence detection.

All dilutions were prepared inside a Class II biosafety cabinet using sterile materials, and volumes of 2 ml were loaded into the quartz flow cells to be measured with the I-CYT. The prepared samples were also cultured in agar plates following the conditions and methods previously described, in order to quantify the microorganism's concentration in the samples through colony counting.

E. coli is an elongated microorganism of about 2 µm in length. *L. pneumophila* is also elongated, yet about half the length (1 µm). *S. cerevisiae* is a yeast microorganism of round shape and 5 µm in size. The phytoplankton microorganisms used were saltwater diatoms with a known size of approximately 14 µm; they have a natural fluorescence emission (autofluorescence) at a wavelength of 610 nm when excited at 488 nm. Since the excitation wavelength spectra of FITC and autofluorescence overlap, one can capture them at the same time and differentiate FITC-labeled *E. coli* and auto-fluorescent phytoplankton. The diatoms were provided by Marine Eco Analytics (MEA-NL) and the *S. cerevisiae,* by Sigma-Aldrich Spain.

Fluidic system for sample concentration

In order to enhance the performance, particularly the sensitivity (lowest detected count) of the I-CYT, a fluidic system was designed. This system comprises a barometric pump and a hollow fiber membrane filter CellTrap™ to concentrate the microorganisms suspended in a large volume and elute them into the 2 ml volume for the quartz flow cell. Three low concentration samples were prepared using the fluidic system as explained below.

First, 1 ml volumes of 10^4, 10^3 and 10^2 cells per ml of *E. coli* in PBS dilutions were added to independent screw cap bottles with deionized water to make a total volume of 500 ml, resulting in *E. coli* concentrations of 20, 2 and 0.2 cells per ml, respectively. The bottles were sealed with a pressurized cap with an input from the barometric pump and an output towards the Cell-Trap™ membrane filter. The filter comprises a set of 0.2 µm hollow fiber membranes which trap the particulates passing through and free the filtered water down one end. Once the entire volume has passed the filter, all the particulates will be trapped inside the membranes and can be eluted into a chosen volume using a Luer tip syringe. After concentration and elution to the 2 ml volume, the virtual concentrations of the three samples become 5000, 500 and 50 cells per ml. Figure 3.3 displays the fluidic system at both stages (concentration and elution). The concentration step represents the initial volume leaving the bottle and passing through the CellTrap™ hollow fibers before the waste is collected in a second bottle. The elution process consists in using a syringe to recover the trapped microorganisms into a smaller volume of 2 ml.

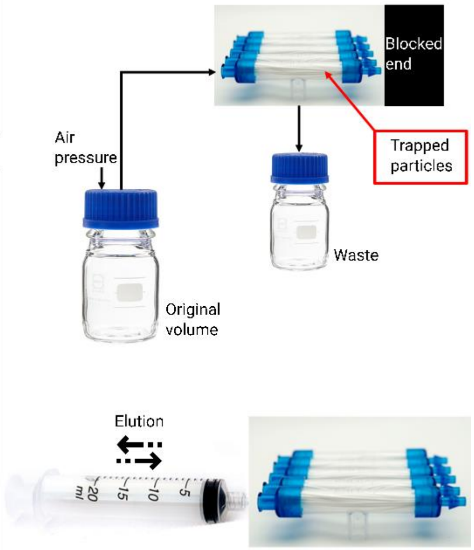

Figure 3.4: Schematic of a fluidic system comprising a barometric pump and a hollow fiber membrane filter CellTrap™ to concentrate the microorganisms suspended in a large volume and elute them into the 2 ml volume for the quartz flow cell. The schematic shows the concentration and elution steps of the process.

3.3. Experimental results.

The following compilation of results demonstrates the capabilities of the I-CYT in measuring and analyzing a variety of waterborne microorganisms over a wide range of concentrations, in both label-free and fluorescent modes.

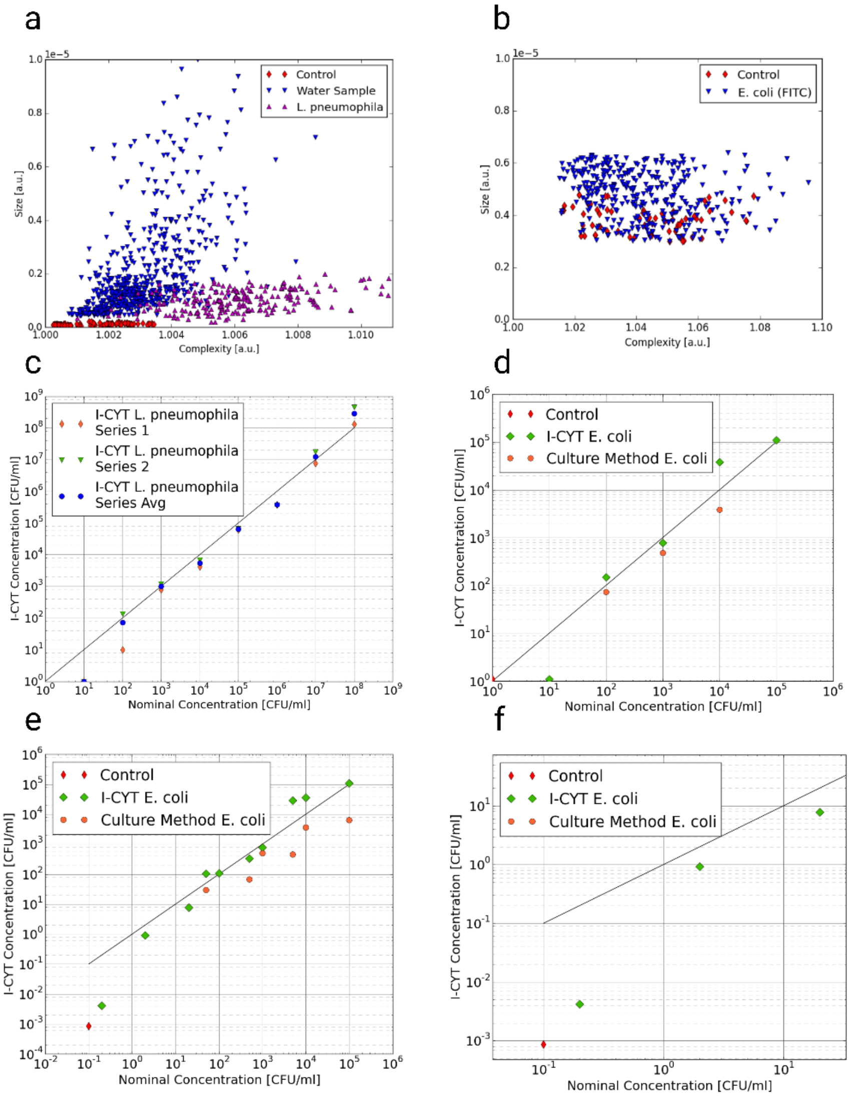

Figure 3.5: Detection and quantification of waterborne microorganisms with the proposed I-CYT. (a) Label-free detection of an L. pneumophila serial dilution in PBS and a water sample taken from cooling towers; (b) Fluorescence detection of the FITC-labeled E. coli suspended in the contaminated cooling tower water sample; (c) Counting of L. pneumophila for (a); (d) Counting of the FITC-labeled E. coli for (b); (e) Results after sensitivity enhancement through the fluidic CellTrap™ concentrator; (f) Zoom of a specific area. All the concentration

measurements (d–f) are compared to the standard microbiological culture.

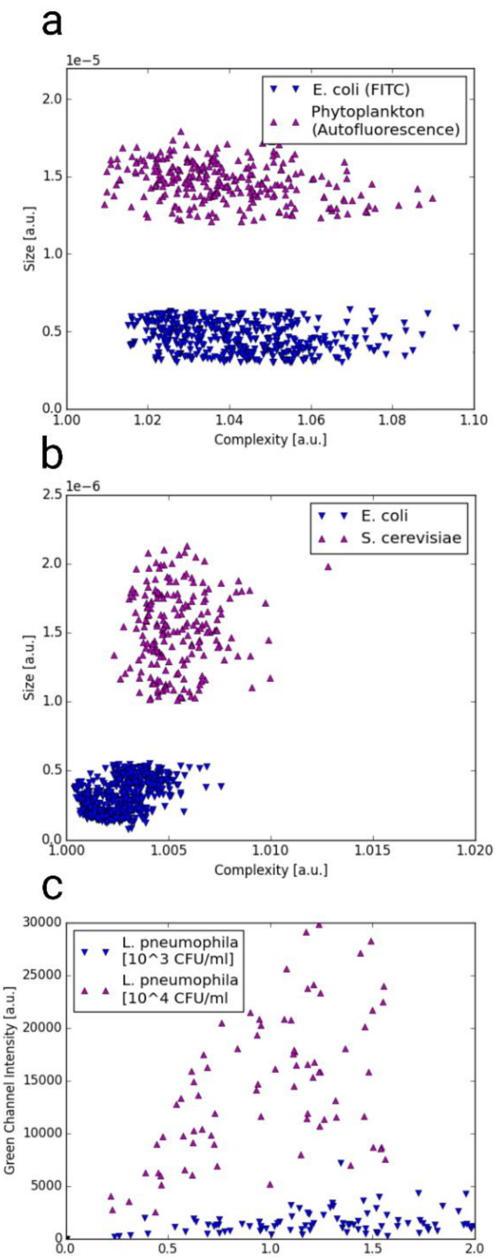

Figure 3.6: (a) FITC-labeled E. coli compared to phytoplankton. (b) Label-free E. coli and S. cerevisiae. (c) Different concentrations of L. pneumophila.

The detection of the microorganisms can be conveniently represented using a dispersion graph – size versus complexity (Figures 3.4a, b and 3.5a, b) – and a concentration graph – size versus concentration (Figure 3.5c). Each point on the dispersion graph corresponds to an observation of these parameters in a single sub-image. By further processing the signal, estimates of the concentration of different waterborne microorganisms can be measured and compared to the control sample of PBS as a baseline (microbiological charge zero). The accuracy of the concentration measurements using the proposed I-CYT is within the 0.5 log when compared to nominal data and microbiological culture results (Figures 3.4c–f). Figures 3.4d and e also display the correlation coefficients (r) between the I-CYT concentration and the microbiological culture, with correlations of 0.9966 and 0.9386 calculated by Pearson’s correlation coefficient.

Figure 3.5a displays the label-free detection of an *L. pneumophila* serial dilution in PBS and a water sample taken from cooling towers with unknown microbiological charge, in contrast to the control sample (PBS). The water from the cooling towers was then spiked with FITC-labeled *E. coli* microorganisms. Figure 3.5b shows the corresponding fluorescence detection results where FITC-labeled *E. coli* microorganisms are characterized in complexity and size, similarly to the *L. pneumophila* samples. Due to the fluorescence labelling and optical filtering, the *E. coli* microorganisms are clearly differentiated from the cooling tower debris. Figure 3.4c displays the counting of *L. pneumophila* for Figure 3.4a, with each dilution measured twice - two series, 1 and 2, together with their average (series Avg). In all cases, the measured value on the vertical axis can be compared with the nominal concentration of the sample on the horizontal axis (no culture results were available for these measurements).

Figure 3.4d shows the concentration of FITC-labeled *E. coli* compared to measurements obtained by the standard microbiological culture of the captured dilutions. Figure 3.4e displays the results after the sensitivity enhancement through the fluidic system and Cell-Trap™ concentrator. The initial volume of 500 ml was reduced to 2 ml by maintaining the same amount of biological charge. This improved the concentration detection limit of the entire system from 50 cells per ml, down to 0.2 cells per ml. Figure 3.4f zooms in on a specific region for further detail. These results validate the I-CYT as a tool to quantify the microbiological charge of waterborne microorganisms.

Finally, in order to demonstrate the capability of the system in identifying and differentiating microbiological populations with a difference in size larger than 3 µm (about pixel size), a new set of samples was measured and processed. *S. cerevisiae, E. coli* and *L. pneumophila* were captured on a label-free configuration, and FITC-labeled *E. coli* and phytoplankton on a fluorescent configuration (Figure 3.5).

E. coli dilutions were labeled with FITC, emitting at 519 nm, and phytoplankton autofluorescence, at 610 nm. Differentiation of these two fluorescence emissions in the I-CYT simply involves placing the appropriate filter for the target fluorescence signal and processing the image using the RGB components of the CMOS sensor with the Bayer filter. By processing the red channel signal, the phytoplankton microorganisms can be detected and analyzed in complexity and size, while the green channel can do the same for the FITC labeled microorganisms (*E. coli* in this case). Figure 3.5a displays the complexity versus size of FITC-labeled *E. coli* microorganisms compared to phytoplankton. *E. coli* microorganisms are known to have a size of around 2 μm, while the phytoplankton diatoms in this sample had a size of around 14 μm.

Using the I-CYT in a label-free configuration, unlabeled *E. coli* and *S. cerevisiae* samples were detected, processed and analyzed. *S. cerevisiae* is a type of yeast with an average particle size of 5 μm. Figure 3.5b shows the complexity and size parameters of the two samples. Samples with a small or no size difference can be differentiated by mapping them with an alternative set of parameters (for instance, complexity versus concentration). For example, Figure 3.6c shows the intensity versus size dispersion for two *L. pneumophila* samples with different concentrations (10^3 cells per ml and 10^4 cells per ml).

3.4. Conclusions

In this chapter, an I-CYT optical reader based on the detection of the optical Fourier transform particulate samples was validated for the measurement of waterborne microorganisms. The sample capture and analysis in the spatial frequency domain have shown an increase in FOV (>24 mm^2) and DOF (≈1 mm) compared to classical imaging techniques. When combined with an ad-hoc fluidic system, these allow the I-CYT to reach a detection level as low as 0.2 cells per ml and analyze hundreds of milliliters of samples in a single capture. In addition, the capacity to differentiate microbial populations by size, complexity, fluorescence emission and concentration is highly suitable for multi-target analysis. The label-free capability is of particular interest for rapid detection of microorganisms. The potential of the I-CYT in industrial applications has been demonstrated by identifying, quantifying, and differentiating waterborne microorganisms of high environmental and societal interest, such as *E. coli*, phytoplankton, *L. pneumophila* and *S. cerevisiae*. As a lower cost alternative, the I-CYT has the potential to replace high-end and large instrumentation with comparable sensitivity and a large dynamic detection (concentration) range, especially where in situ and immediate countermeasures are required. This is the case, for example, for remote areas which lack infrastructure and laboratories where analyses are typically performed.

4

Ballast water monitoring applications of Fourier imaging cytometry

The information, text and figures in this chapter have been adapted, under the terms of the Creative Commons Attribution Non-commercial license, from the original publication: "CMOS based image cytometry for detection of phytoplankton in ballast water", J. M. Pérez, M. Jofre, P. Martinez, M. A Yáñez, V. Catalan, A. Parker, M. Veldhuis, and V. Pruneri. Biomedical Optics Express, 2017, Vol. 8, Nº 2, 1240.

4.1 Introduction. Application-specific challenges.

In the previous chapters, we introduced an optical reader based on angular spatial frequency processing and incorporating consumer electronics complementary-metal-oxide semiconductor (CMOS) image sensor array for the detection of waterborne microorganisms [32].

By leveraging such optical reader, we present in this chapter an industrialized variation that focuses on designing, building and validating such device in a field-portable form for rapid detection and quantification of microorganisms in ballast water (BW). Furthermore, this device was also applied to analyze the effects of ultraviolet and chlorine ballast water treatment systems (BWTS).

To frame the motivation for this experiments and industrial validations, we must take a closer look at current environmental challenges that somehow create the need for devices such as our image cytometer. Globalization has become a primary driver of one of the most prevalent forms of environmental degradation: marine invasive species. As trade continues to flourish, bio- invasion is becoming more difficult to handle [33]. Among the marine invasive species, microorganisms carried in BW can easily spread into a new habitat. This can generate a potentially devastating impact threatening the ecosystem and human activities [34]. Of the microorganisms, some species of phytoplankton can cause illness to mammals, fish, corals and other marine organisms.

BW refers to the water in the tanks of ships used to increase their stability, which is discharged into the ocean after long journeys. While doing so, it also introduces numerous invasive organisms to the ecosystem of discharge [35]. BW on ships is considered to be the most important vector in dispersing invasive species throughout the world [36] as more than 150.000 metric tons of fresh/marine water can be pumped in or out in only one ballast / de-ballast operation [37]. In response to the threats from continued introductions of aquatic invasive species, the United Nations International Marine Organization (IMO) adopted the International Convention for the Control and Management of Ships' Ballast Water and Sediments [38]. The IMO regulation sets procedures to discharge BW in ports, to minimize the spread of invasive and pathogenic organisms. Its compliance requires testing for phytoplankton, zooplankton, toxicogenic *Vibrio cholera (V. cholera)*, *Escherichia coli (E. coli)* and intestinal *Enterococci* upon discharge of the BW in the harbor.

BWTS represent a way of disinfecting BW in order to reduce the number of organisms to low risk levels for the ecosystem and human health; BWTS are either on board or port-based systems which are able to clean all BW before it is released into the harbor [39]. The main on board and port-based treatment technologies used today are ultraviolet (UV) sterilization [40] and chlorine electrolysis [41].

Collaborative efforts between biologists, physicists, engineers, chemists and material researchers have yielded novel strategies in understanding complex marine ecosystems. A variety of analytical methods have been used to identify changes in populations of marine organisms ranging from large to small scale like: remote spectrometry from satellites and airplanes, in situ spectrometry, (laser)-induced fluorescence, microscopy and flow cytometry [42].

Other biosensing systems for on-board analysis of BW and quantification of the living organisms have been developed and reported. For example, sensors based on molecular and genetic engineering methods [43], [44]; others relying on the photosynthetic properties, universally present in phytoplankton [42], [45]. In previous chapters, we introduced our technology of spatial frequency processing optical reading and how it could be applied to industrial settings such as microorganism detection in cooling towers or bathing waters. Through the identification of the BW water monitoring challenge, we decided to adapt our technology and validate it in this setting, furthering the impact of our research.

4.2 Experimental realization.

Adaptation of the Image Cytometer

The focus of the adaptation was on taking a laboratory setup and turning that into a portable device without sacrificing any of its features or performance. It was an engineering effort which involved a certain level of innovation into the optical setup and processing software to assure the performance in an industrially relevant environment.

Our image cytometer is an opto-mechanical reader comprised of a CMOS image sensor array as a detector and a collimated bandlimited light emitting diode (LED) source centered at an excitation wavelength of 466nm. The collimated beam illuminates the sample volume, which is contained in a disposable Poly (methyl methacrylate) (PMMA) cuvette with a capacity of up to 3ml. The use of a PMMA cuvette was one of the steps taken towards industrializing our optical device. Previous experiments used quartz cuvettes to contain the sample because of the optical characteristics of quartz. Using PMMA implied that our software now needed to account for fabrication imperfections. Continuing in the optical path of our device, an interference optical filter allows the simultaneous detection of two fluorescent channels centered at 512nm and 630nm, respectively. Phytoplankton species exhibit auto-fluorescence in wavelengths above 610nm, because of their chlorophyll. This fluorescence can be used for quantification, but as we'll see, it can also be used for measurements of the vitality (defined in this scope as the capacity of the phytoplankton organisms to reproduce).

In the interest of portability of the device, we replaced the optical lens in the laboratory setup for a parabolic mirror, for the purposes of performing the optical Fourier transform of the sample volume. Parabolic mirrors can act as optical lenses with a given reflective focal length (RFL) at a specific off-axis angle. For our device, we used a parabolic mirror with RFL 50.8mm and off-axis angle of 90 degrees. The mirror was placed after the filter, to collect the light field from the sample and projecting its optical signal, after the Fourier transform, onto an array of microlenses. The microlenses physically sample the incoming beam and focus it onto different areas on the CMOS image sensor array. The combination of the optical transforming element and the microlenses array allows for the detection of the organisms in the sample in such a way that they can be counted (based on fluorescence emission) and discriminated by size (by analyzing the sub-images patterns).

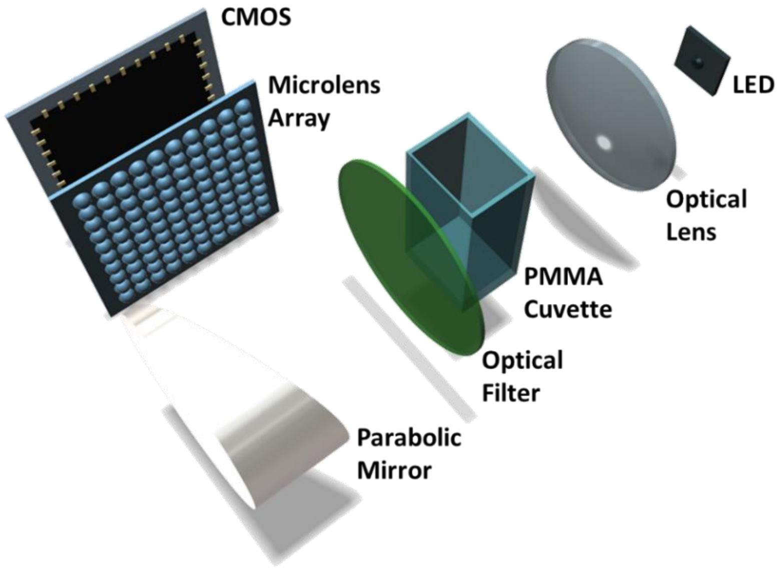

Figure 4.1: schematic of the opto-mechanics of our industrially adapted image cytometer.

The complete image cytometer combines fluorescence detection with Fourier optics for an analysis of the sample in terms of concentration, vitality and size. Figure 4.1 shows a schematic of the opto-mechanics of our device. Figure 4.2 show brightfield captures of a buffer samples (a) and a particulate sample (b) using the image cytometer. These images correspond to the formatted Fourier transform, which can in turn be analyzed for quantification of particles and size information. For the size of the particle, each lobe of the microlens is analyzed independently in terms of the spatial bandwidth product (SBP) of our optical system, detailed in chapter 3.

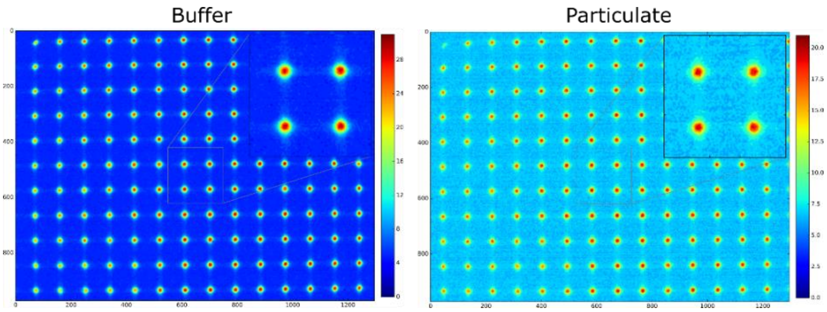

Figure 4.2: brightfield captures of a buffer samples (a) and a particulate sample (b) using the image cytometer. These images correspond to the formatted Fourier transform, which can in turn be analyzed for quantification of particles and size information.

For the implementation of our device, we also enhanced the detectable range of intensities of our system by studying the detecting principles of CMOS sensors and introducing a high dynamic range (HDR) capturing algorithm. The CMOS image sensor, being a transistor-based technology, has a sigmoidal response to intensities. It has a sub-saturation region for low intensity (corresponding to low fluorescence signal or low concentration), a saturation level at high intensity (concentration) and a linear region in between. By combining the CMOS response with an HDR algorithm, we are able to detect concentrations through a range of as large as 50dB.

Sample preparation, testing and processing

The dynamic range of our device was determined by means of serial dilutions of two phytoplankton species: *Tetraselmis* (14μm in cell diameter) and *Nannochloropsis* (5μm in cell diameter).

The next step was testing the functionality of the system by measuring and quantifying phytoplankton species in samples from fresh and marine waters (BW samples), that being our industrial application. Furthermore, we tested the capacity of our device on measuring water samples collected from full scale BWTS by passing these water samples subjected to UV sterilization or chlorine electrolysis. Phytoplankton numbers were quantified, and the vitality of the cells was measured before and after the treatment.

For comparison, field samples were analyzed with a standard flow cytometer (Beckman Coulter EPIC-XL-MCL) [46]. The vitality of the phytoplankton was measured as the efficiency of the photosynthetic system of the phytoplankton [47]. For this analysis the WALZ-Water-PAM was used measuring bulk fluorescence properties of the phytoplankton [48].

The semi-quantification of organisms in cells per ml was achieved by transforming the fluorescence intensity with a 4 parameter logistic (4PL) regression [49] (see equation 4.1), where, (A, B, C, D) refer to the four parameters of the regression, with values ($2.17\text{x}10^8$, $1.31\text{x}10^3$, $3.33\text{x}10^7$, $4\text{x}10^2$) respectively, and I_{CYT} refers to the fluorescence intensity. The use of a 4PL regression describes our biosensing system more suitably than a linear regression. The model has a maximum (D) and a minimum (A) built into the equation, which better describes biological systems. Parameters (C) and (B) act as offset and slope values respectively.

$$Concentration\left[\frac{cells}{ml}\right] = C \cdot \left(\frac{A - D}{I_{CYT} - D}\right)^{1/B} \tag{4.1}$$

For the vitality index measure, the light source in the system was controlled by a pulse width modulation (PWM) signal that allowed for the detection of the minimum and maximum fluorescence of the organisms. For the maximum fluorescence (F_m) the sample was excited by a PWM signal with 50% duty cycle and 5ns period. For the minimum fluorescence (F_0), the sample was excited by a PWM signal with 50% duty cycle and 10µs period. The sample was captured under both conditions, thereby obtaining the experimental values of F_m and F_0. By measuring and comparing maximum and minimum fluorescence, we can identify the vitality of the organism. In the minimum fluorescence excitation mode, we allow the microorganism to reach the excitation state and back to its stable state several times through our capture, as the time-off of the light source is orders of magnitude longer than the state changes of the microorganism. In the maximum fluorescence excitation mode, we try to maintain the organism at an excited stage (to the limit of what our electronics allows us). As average minimum and maximum fluorescence approach each other, it is indicating that the microorganism has lost its capacity to reproduce [48]. The vitality index was calculated as follows:

$$Vitality = 1 - \frac{F_0}{F_m} \tag{4.2}$$

To test our newly adapted device we used controlled cultures of *Tetraselmis* and *Nannochloropsis* for laboratory test and system calibration, before taking the device the field. Both *Tetraselmis* and *Nannochlorpsis* were taken from concentrated stocks of green microalgae, the former of the *Tetraselmis chuii* species and the latter of the *Nannochloropsis oculata* species; both purchased from Acuinuga (A Coruña, Spain). For the system validation in-field (BW environment), samples of both marine and fresh water were measured; the marine and freshwater samples were subjected to BWTS chlorine electrolysis; the freshwater samples were also exposed to BTWS UV sterilization.

Dilutions of the samples (1/10 v/v) were made in a marine water medium filtered under 0.2µm with a hollow membrane filter CellTrap™. The *Tetraselmis* culture media contained high levels of large sized debris, especially at the highest concentration measured ($1/10^2$). To avoid the absorption of excitation light from said debris material, a cell extraction protocol was performed to separate the *Tetraselmis* cells at this concentration. The protocol consisted on the centrifugation of the sample at 1500 revolutions per minute (rpm) for 10 minutes at 4°C; which would effectively separate the larger debris from the *Tetraselmis* cells. After centrifugation the supernatant was recovered and measured with the device.

Freshwater samples were collected from Lake Ijssel (The Netherlands) and marine water samples from brackish water off the coast of Den Oever (Dutch Wadden Sea, The Netherlands). One of the freshwater samples was concentrated from its original volume of 400ml down to 3ml using CellTrap™ membrane filters. The intensity recorded from our optical reader was corrected considering the eluted volume (3ml eluted from the filter), original volume (400ml originally sampled) and recovery rate (RR). The recovery rate of the CellTrap™ (RR) is 0.98 as reported by the manufacturer. This correction allowed us to compare our results to those of the flow cytometer.

In the case of the UV BWTS, the treatment included two different steps. The first consisted in exposing the water sample to UV light followed by a 24-hour holding; the second one included an additional UV exposure step after the 24-hour holding period.

4.3 Experimental results.

The first step for our experiment was to build the newly designed filed-portable adaptation of our I-CYT. After testing the adapted setup in the laboratory, we build our beta prototype, which was then used to measure all samples. Figure 4.3 displays the process of building this beta prototype.

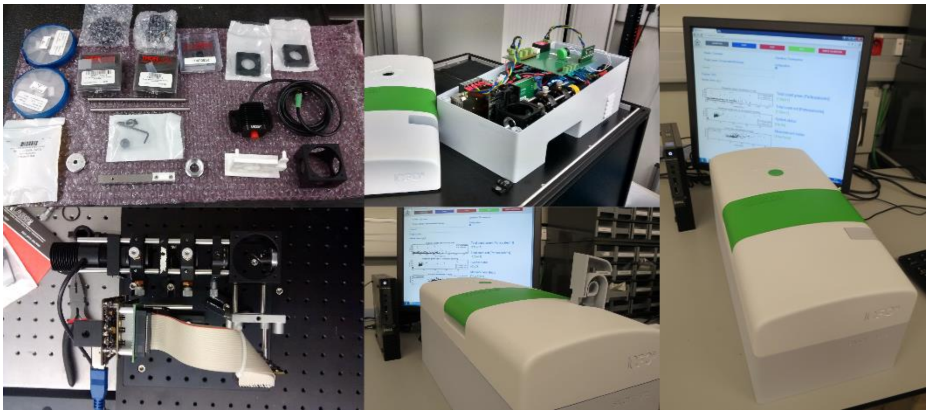

Figure 4.3: process of building the beta prototype of the industrially adapted image cytometer.

We then measured unialgal cultures of *Tetraselmis* and *Nannochloropsis* to evaluate the linearity, repeatability, reproducibility and LOD of our device, these measurements took place in a controlled laboratory environment, simulating the testing protocols of the in-field measurements that followed. We then took our prototype to the coast of Den Oever (Dutch Wadden Sea, The Netherlands) for the measurements of fresh and marine water samples to validate our device in an industrially relevant environment. We correlated our results with a flow cytometer as a standard method.

Detection of *Tetraselmis* and *Nannochloropsis*

For the initial tests two independent series of both *Tetraselmis* and *Nannochloropsis* were measured over five orders of magnitude in 1/10 (v/v) dilutions. Each sample was measured three times for repeatability and intra-assay evaluation. The serial dilutions allowed us to demonstrate the linearity of our device and its limit of detection (LOD). The comparison between independent series evaluated reproducibility (inter-assay testing).

Figure 4.4 compiles the results for the *Tetraselmis* and *Nannochloropsis* samples measured. For the *Nannochloropsis* results, at the highest concentration measured (10^{-3} dilution), our device reports a concentration of $3{\cdot}10^3$ cells/ml; the lowest concentration detected was

6 cells/ml, at a 10^{-6} dilution. One more dilution was measured (10^{-7}) but went undetected as it was on average below the baseline of the device. Our baseline is taken from multiple measurements of blank samples (clean buffer). For the *Tetraselmis* at the highest concentration measured (10^{-2} dilution), our device reports a concentration of 10^{4} cells/ml; the lowest concentration detected was 18 cells/ml, at a 10^{-5} dilution. One more dilution was measured (10^{-6}) but went undetected as it was on average below the baseline.

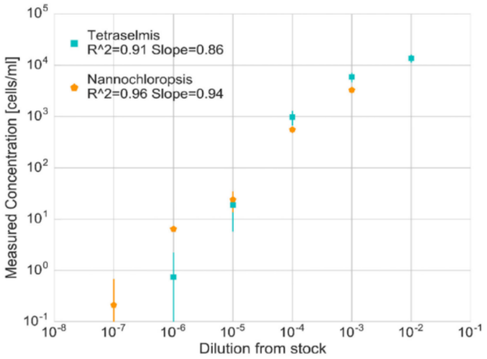

Figure 4.4: results for the Tetraselmis and Nannochloropsis samples measured.

Table 4.1 shows the intra-assay and inter-assay logarithmic deviations for both species at all concentrations measured. On average, our device exhibits an intra-assay deviation of 0.282 and an inter-assay deviation of 0.1; this translates into an accuracy between 0.7 and 0.5 log. For comparison, when using a microscope, the *Nannochloropsis* stock showed a concentration of $7{\cdot}10^{6}$ cells/ml, while the *Tetraselmis* stock of 10^{6} cells/ml.

To validate the LOD, a total of 10 independent samples per organism were measured at the lowest detected concentrations; 6 cells/ml for *Nannochloropsis* and 18 cells/ml for *Tetraselmis*. For these measurements, the *Nannochloropsis* samples had an inter-assay deviation of 0.38. The *Tetraselmis* samples had an inter-assay deviation of 0.20. Deviations are taken as standard deviation of the base 10 logarithm of the observations.

Table 4.1: intra-assay and inter-assay logarithmic deviations for both species at all concentrations measured.

	DILUTION FROM STOCK	INTRA-ASSAY DEVIATION		INTER-ASSAY DEVIATION
		Series 1	Series 2	
NANNOCHLOROPSIS	10^-3	0.08	0.01	0.06
	10^-4	0.02	0.07	0.05
	10^-5	0.18	0.12	0.20
	10^-6	0.11	0.51	0.41
	10^-7	0	0.59	0.47
TETRASELMIS	10^-2	0.06	0.08	0.07
	10^-3	0.07	0.04	0.08
	10^-4	0.08	0.16	0.14
	10^-5	0.26	1.11	1.32
	10^-6	1.91	0.18	1.49

4.3.1. Industrial applications. Microbiological detection in ballast water treatment systems.

Unlike cultures, samples collected from the field consists of a larger variety of phytoplankton differing in size and chlorophyll content. These samples were therefore filtered over a 10-micrometer net as to split our sample into two size windows (ranges). The selection of this 10μm threshold was intentionally chosen as to meet the standards of the IMO for the analysis of BW. Figure 4.5 shows the comparison between the concentration in [cells/ml] as measured by both platforms (our device and a flow cytometer) below and above the 10μm size threshold. Both devices gave very close results, with a deviation of

0.05 and 0.14 for the window below and above threshold, respectively.

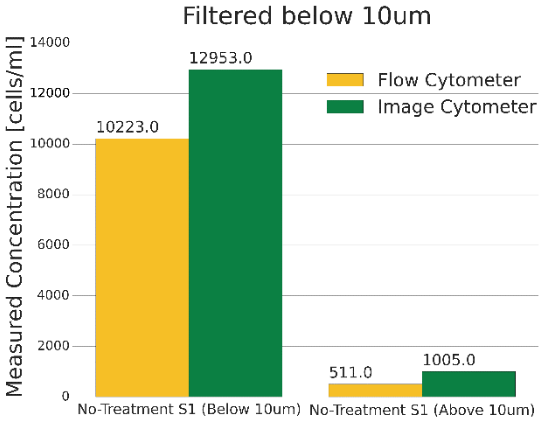

Figure 4.5: comparison between the concentration in [cells/ml] as measured by both platforms (our device and a flow cytometer) below and above the 10μm size threshold.

Figure 4.6 displays the marine water samples measured before and after the disinfection step using a chlorine electrolysis BWTS. The phytoplankton population was quantified in the two windows of interest; larger (a) and smaller (b) than the 10µm threshold. The chlorine resulted in a reduction of the phytoplankton population in both regions. This can be especially noted in samples 1 and 3, where the decrease in cell numbers was one order of magnitude with respect to untreated samples. In sample 2 the BWTS has a lower impact: the reduction was only a 50% numerical reduction below the size threshold and even smaller above the 10µm size range.

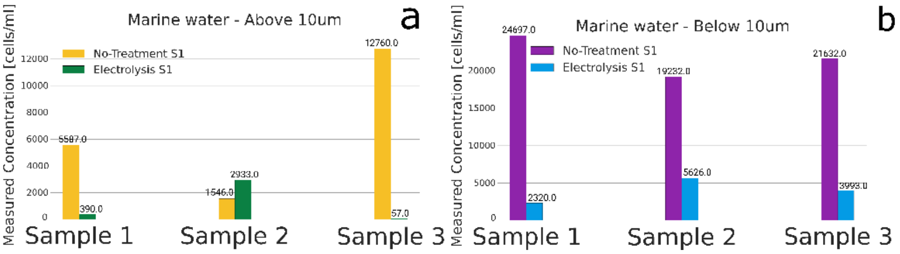

Figure 4.6: marine water samples measured before and after the disinfection step using a chlorine electrolysis BWTS. The phytoplankton population was quantified in the two windows of interest; larger (a) and smaller (b) than the 10µm threshold.

Figure 4.7 displays the results of concentration and vitality for freshwater samples before and after three different treatment protocols of the BWTS (chlorine electrolysis, UV sterilization with 1-day holding, and UV sterilization with one day holding and a second UV exposure after holding). A total of six samples were tested; samples 1 through 3 had (no treatment), and samples 4 through 6 with the three different BWTS protocols. The vitality index of non-treated samples ranged between 0.6 and 0.77, for both size ranges.

Samples 2 and 3 in Fig. 4.7 came from the same original bulk sample, with the difference that sample 3 was concentrated from 400ml down to 3ml (CellTrap^{TM}). This shows a strong performance when combining our device and the CellTrap^{TM} filter in measuring concentrated samples. The deviation in concentration between samples 2 and 3 was 0.01 with the filter presenting a RR of 0.96 (in line with the performance characteristics of the CellTrap™) (Fig. 4.7 a), proving the efficacy of the filter and the reproducibility of our reader.

Sample 4 in Fig. 4.7 was treated with chlorine electrolysis, the results show a decrease in cell numbers of at least one order of magnitude (Fig. 4.7 a and 4.7 b), analogue to the effects of BWTS in marine water samples (Fig. 4.6). The vitality index of the sample after the treatment was 0.01 below the size threshold and 0.08 above it (Fig. 4.7 c and 4.7 d).

Finally, samples 5 and 6 show the results after UV sterilization and 1-day holding (sample 5), and second UV exposure after holding (sample 6). Both concentration and the vitality index were reduced to similar levels in both treatments and for all size regions, data corroborated by the flow cytometry results. The second UV- disinfection treatment after 1 day holding time did not differ significantly from the first treatment, therefore the increased efficacy of the second treatment can be considered as minor.

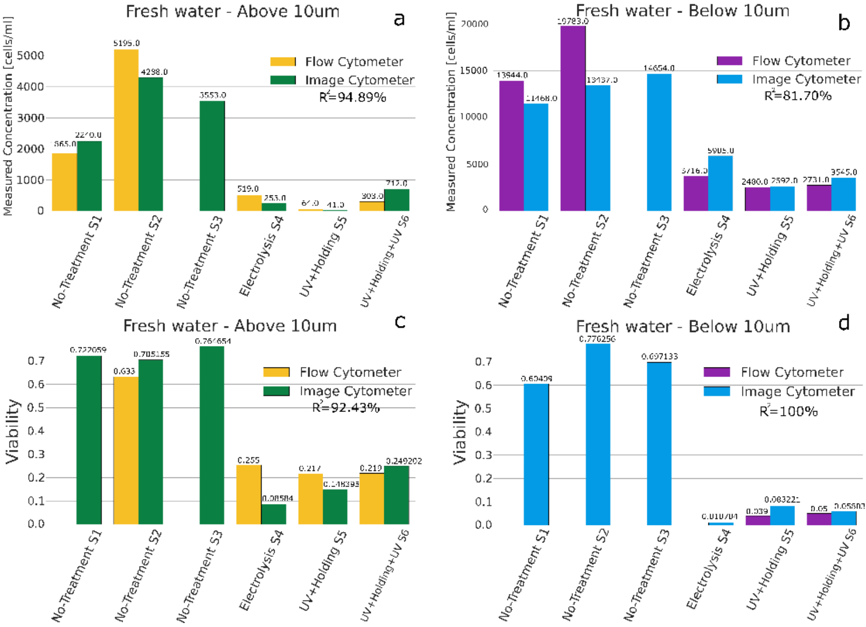

Figure 4.7: results of concentration and vitality for fresh water samples before and after three different treatment protocols of the BWTS (chlorine electrolysis, UV sterilization with 1-day holding, and UV sterilization with one day holding and a second UV exposure after holding). A total of six

samples were tested; samples 1 through 3 had (no treatment), and samples 4 through 6 with the three different BWTS protocols.

4.4 Conclusions.

In this chapter we reviewed the industrial adaptation and validation of our technology. We went through the different enhancements in our technology that had to be introduced in this first industrialization approach of our technology. We built a beta prototype of our optical reader, as a field-portable fully operative device. We validated its performance in the laboratory, simulating an industrial environment. We then took our system for in-field measurements and demonstrated its capacity in an industrially relevant environment. We have validated the capacity of this prototype to analyze phytoplankton in fresh and marine water environments. The results and their reproducibility demonstrated the high performance of this prototype for the quantification of phytoplankton, both inside and outside a laboratory environment.

In the present study the focus has also been on quantifying the efficacy of BWTS. To this end, by using pulse width modulation (PWM) of the excitation light source, accurate measurements of vitality of the phytoplankton were achieved. Thereby being able to evaluate the efficacy of the BWTS tested.

The experiments clearly indicate that our prototype has comparable performance to standard flow cytometry equipment, and given its portable compact form, is a very promising solution for the analysis of BW and prevention of spreading of invasive species.

5

Surface cytometry

The information, text and figures in this chapter have been adapted, under the terms of the Creative Commons Attribution Non-commercial license, from the original publication: "Surface cytometer for fluorescent detection and growth monitoring of bacteria over large field-of-view", Rafaël Sibilo, Juan Miguel Pérez, Felix Tebbenjohanns, Cedric Hurth, and V. Pruneri. Biomedical Optics Express, 2019, Vol. 10, Nº 4, 2101.

5.1 Introduction. Application-specific challenges.

There is a growing need for low-cost methods and compact biosensors, particularly for point-of-care (POC) applications where resources in terms of space and funds are often very limited. Being able to monitor the growth of bacterial pathogens precisely is of utmost importance in a large number of clinical and environmental situations as well as in food quality control. In many cases, the growth of biofilms on a surface is a starting point for contamination [1-3]. Indeed, the first step of microbial biofilm formation is the adhesion of a few cells to a surface [1], which is why many state-of-the-art sensors for biofilm detection rely on surface measurements. Multispecies biofilms have shown even stronger resistance to antibiotics than when in suspension [3], which is another strong reason for developing accurate methods to measure biofilm formation and take preventive action in the early stages of the biofilm growth.

5.2 State of the art. Devices and techniques for bacteria detection on surface.

When reading a biological signal, there are many options available for signal transduction. The design of the sensor is primarily driven by the desired specifications, such as sensitivity and specificity, and the final environment in which it will operate (in-field or laboratory). These are, to an extent, scientific constraints but the final choice of a sensor will ultimately be affected by economic considerations. Recently, a few elegant approaches have been published with magnetoelastic biosensors that can be directly placed in contact with the food surfaces to be analyzed [4-6]. This a great advantage because it reduces sample preparation time and enables direct in situ measurements. However, the microfabrication of the sensor is complex and costly and the limit-of-detection (LOD) remains rather high. Electrochemical sensors offer the clear advantages of low-cost and easy integration but often require electrode surface modification [7] in order to provide LOD values that can be relevant in real conditions, namely lower than 100 cells/ml. Spectroscopic measurements by Raman scattering or surface-enhanced Raman scattering (SERS) can lead to multifunctional sensors with high specificity [8] and even direct in situ measurements [9]. However, the necessity to fabricate nanostructured surfaces to significantly enhance the detected signal and achieve competitive LOD values, combined with the complex signal analysis, have significantly restrained their widespread adoption. Quantitative PCR (qPCR) offers the highest sensitivity and specificity but requires complex efforts for sample collection and preparation [10]. In addition, qPCR is often time-consuming and requires at least 1 hour to complete enough cycles to amplify the DNA to detectable signal levels. Because of the variety of fluorescent dyes [11,12] or fluorescent probes [13] available for bacteria detection as well as strong autofluorescence [14], optical methods centered on the detection of fluorescent signals remain the main type of biosensors developed and adopted in recent years. The challenge here is to design and build a cost-efficient detection setup while maintaining the high sensitivity enabled by the fluorescent probes and allowing multiplexing [15], especially when the device is to be used for in-field measurements. To reduce the cost and the complexity of the device, colorimetric assays have been developed [16] but the low sensitivity (absorbance) often requires amplification of the bacterial DNA material in order to reach significant LOD values [16].

For the reasons stated above and because our aim is to develop a low-cost portable technology, we designed an optical-mechanical assembly to measure the fluorescence of bacteria labeled with DNA-intercalating dyes such as SYBR Green I. The optical head includes a light-emitting diode (LED) light source and a complementary metal-oxide-semiconductor (CMOS) sensor [17]. A CMOS sensor was chosen because it is a widespread, yet sensitive, image sensor readily available in consumer electronic devices such as smartphones. This would facilitate the industrialization of our device to be easily adapted to low-cost settings, enabling point-of-care applications outside of the laboratory or clinic. More importantly, the key benefit of our approach is to probe a large field of view of about 300 mm^2 thereby decreasing the application specific demand for a small LOD, given that a larger area can be probed in a single measurement. The LOD obtained shows a significant increase on values reported by a similar method concentrating directly on the surface to be probed [7,15]. The device enables real-time growth monitoring because the acquisition time is less than 1 minute per frame. All components used are off-the-shelf with a few customized mechanical parts for added stability. The overall footprint is small, and the weight is kept low for portability and easy field deployment.

Table 1 represents the overall state-of-the-art comparison of our sensor with the other technological approaches reviewed for this study.

Table 5.2: State-of-the-art comparison of biosensors for surface applications. S-CYT refers to our surface cytometer.

Technology	**LoD**		**Time**	**Real**	**Portability**	**Viability**	**Substrate**
	cells/mL	cells/mm^2	**[min]**	**time**			
S-CYT	**--**	**10^4**	**<1**	**Yes**	**Yes**	**Yes**	**Glass**
qPCR	--	10^2	>60	No	No	No	Custom
Colorimetric	10^2	--	>60	No	Yes*	No	Custom
Magnetic	--	10^3	<1	Yes	Yes**	Yes	Direct
SERS	--	10^4	20	No	No	No	Custom

5.3 Device design and implementation.

The optical reader has a total dimension of 20 cm x 20 cm x 10 cm including the controlling electronics and the power supply. It is composed of four main modules: an incoherent light source (LED), an optomechanical assembly, a CMOS image sensor, and controlling electronics. Figure 1 shows the schematics of the optics interfacing, with a sample slide (Figure 1A) and an image of our surface cytometer (Figure 1B) used in the laboratory.

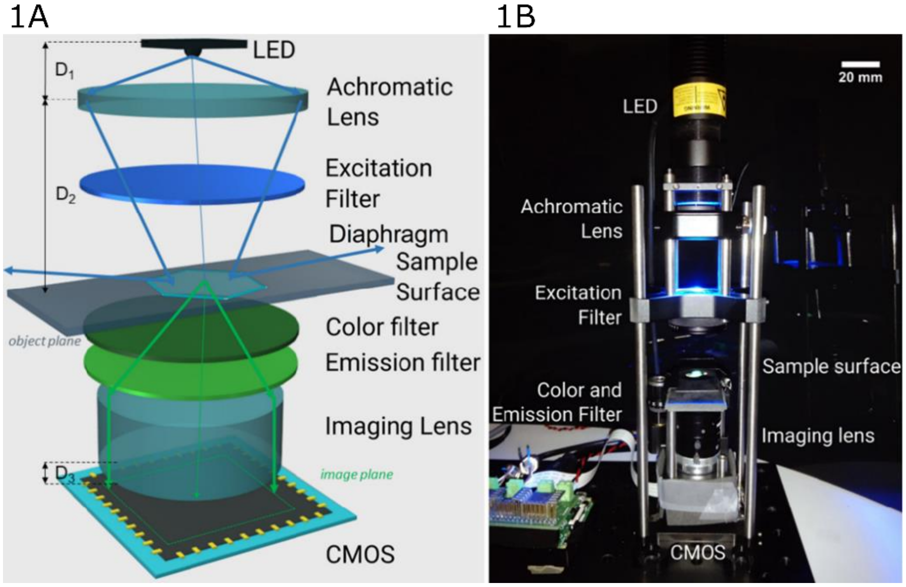

Figure 5.7: shows the schematics of the optics interfacing with a sample slide (Figure 1A) and an image of our surface cytometer (Figure 1B) used in the laboratory.

The light source is a free space high power LED (M470L3, Thorlabs, GmbH), which is band-limited using an interference filter with a center wavelength (CWL) of 466 nm and a bandwidth (BW) of 40 nm (86532, Edmund Optics Ltd.). The optomechanical assembly comprises optical elements mounted on precision holders, creating a vertical optical axis to excite the surface with the light source, collect the emission from the sample and transmit the emitted optical signal to the CMOS detector. The optical elements are assembled as follows, and include: an achromatic lens with a focal of 50 mm, an interference filter with a CWL of 526 nm and a BW of 53 nm (87241, Edmund Optics Ltd.), a green color filter (46053, Edmund Optics Ltd.), and an imaging lens with an effective focal length of 6 mm equipped with a manual focus and an iris (Navitar). An achromatic lens was used to confine the light source onto the target surface (sample). The combination of the interference and color filters allowed for the proper suppression of the excitation wavelength (light source). Even with a high power, non-collimated beam, this combination of filters allowed us to remove the excitation light hitting the surface of the filters at all angles, which improved the signal-to-noise-ratio (SNR) despite a peak transmission coefficient of 70% for the color filter. The imaging lens was used to focus the detection on the surface plane and was arranged to obtain a field of view of 300 mm^2 and a spatial resolution of 280 µm. Since the objective of the sensor is to detect and process surface aggregate information, we increased the FOV while sacrificing spatial resolution. We used a positive 1951 USAF test target (R3L1S4P, Thorlabs, GmbH) for the quantification of the FOV and spatial resolution. The resulting normalized image is shown in Figure 2. The CMOS image sensor is a 4.6-mm diagonal sensor with 3280 x 2464 pixels (Sony IMX219), also known as version 2 of the Raspberry Pi camera module. We removed the lens originally mounted over the sensor.

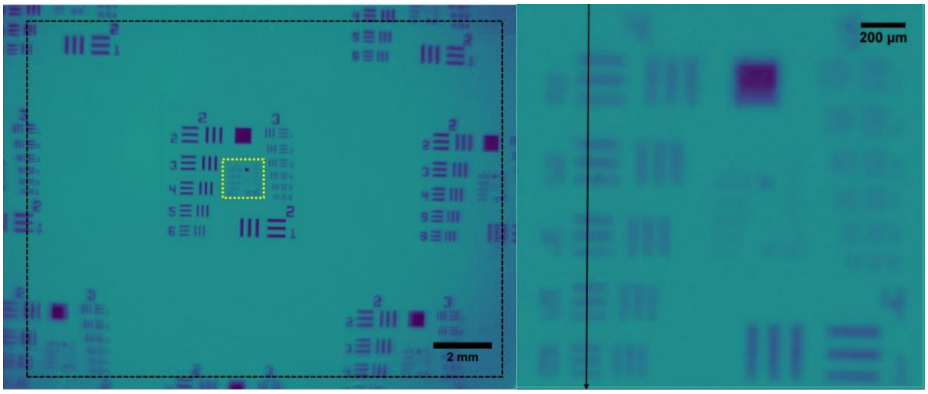

Figure 5.2: Normalized image of the positive 1951 USAF test target (R3L1S4P, Thorlabs, GmbH) for the quantification of FOV and spatial resolution.

5.4 Experimental realization.

Control electronics

The controlling electronics are comprised of a Raspberry Pi 3 Model B, which processes the electronic signal acquired after detection with the image sensor to provide a fluorescence count proportional to the sample emission level. In order to control the camera using Python, a third-party module (picamera) was used. Like most CMOS sensors today, the IMX219 uses a Bayer filter configuration to structure its pixels. Every 2 x 2 block of neighboring pixels contain one red, one blue, and two green pixels. A single capture consists of four two-dimensional arrays with a size of 1640 x 1232 pixels and 10 bits for each pixel. The exposure time and gain of the sensor can also be adjusted using the picamera module. From this raw data, we developed our own software to retrieve only the signal corresponding to the channels of interest (both green channels for the configuration disclosed - see “Bacteria nucleic acid stain” section below) and process it to obtain a single fluorescent count proportional to the aggregated bacteria on the 300 mm^2 surface.

The Raspberry Pi also includes general-purpose input/outputs (GPIOs) to connect miscellaneous electronics. We designed a printed circuit board (PCB) to control the LED. A nominal current of 1A and a forward voltage drop of 3.5V drive the incoherent light source described and a power supply of 5V at 5A feeds the complete system.

Bacteria growth and incubation

To prepare the analyzed samples, *Escherichia coli* (Invitrogen DH5 alpha) was grown at 37ºC in LB Broth medium (Scharlau 02-384-500) with an incubator shaker (Thermo Fisher Scientific MaxQ8000). We controlled the bacterial growth by monitoring the optical density (OD) with a spectrophotometer (Thermo Fisher Scientific Nanodrop 2000c), measuring the absorption at 600 nm. We monitored the bacteria growth over the course of 8 hours. For each time analyzed, an aliquot of the culture was stained and deposited directly onto the reader sensor without further processing. Each aliquot was processed in triplicate and 3 acquisitions were averaged for each measurement.

Bacteria nucleic acid stain

In order to monitor bacteria growth with the surface cytometer, *E. coli* cells were labeled with a fluorescent nucleic acid stain, namely SYBR Green 1 (SG), from a 10,000X concentrate stock solution (Invitrogen S7563) in dimethyl sulfoxide (DMSO). SG has a peak absorption at 490 nm and a peak emission at 520 nm. SG intercalates within double-stranded DNA helixes without specificity. When it is bound to DNA, the fluorescence is increased by several orders of magnitude. 10 µL of SG stock solution was dissolved into 100 µL of phosphate buffered saline (PBS, Sigma-Aldrich P4417). Each 1 mL of sample was treated with 1 µL of SG. Before each measurement, the samples were incubated for 20 minutes at room temperature. For the purpose of growth monitoring, we labeled and measured samples at different OD values, and compared the surface cytometry results to those obtained with the spectrophotometer and a fluorescence microscope (Nikon Ti inverted microscope with Andor iXon camera).

Surface measurement

For the measurements with the surface cytometer, we prepared the surfaces by combining borosilicate cover slips with a thickness of 100 μm (Knittel Glass) with silicon isolators (Grace Bio-labs GBL665301) to confine the sample to an area larger than the instrument FOV. Since our interest was in the aggregated effect of the cells on the surface, signal processing was limited in order to obtain a fluorescence count from the sample. It was correlated to a concentration of bacteria in cells/mm^2 or used to build a complete growth curve similarly to the measurements with the spectrophotometer. For characterization and comparison purposes, we also imaged the samples with a fluorescent microscope.

5.5 Experimental results.

The main drive of the study was to compare the generation of a growth curve using our low-cost platform with standard accepted methods such as absorbance (turbidity) measurements and fluorescence microscopy.

5.5.1. Reference growth curve using absorbance measurements.

One of the most standard methods for measuring bacterial growth is by using absorbance measurements. Figure 3 shows the growth curve obtained by averaging the curves measured over various experiments carried out over several weeks growing *Escherichia coli* in liquid LB at 37 °C and collecting an aliquot (50 μL) at the indicated times to perform the absorbance measurement. The data is reported in terms of changes in the optical density (OD), which considers various phenomena including scattering and absorption, which modify the intensity of the light transmitted by a medium with respect to the incident light flux. Bacterial growth parameters such as the lag time (T*lag*) or the recovery time to reach a significant cell-division rate after being transferred to a new environment, and the absolute growth rate (k_Z), were determined by fitting the data to the Gompertz-Zwietering model [19,20].

$$OD(t) = B_G + A_G \cdot \exp\left(-exp \cdot \left(\frac{ek_Z}{A} \cdot (Tlag - t) + 1\right)\right) \qquad (5.1)$$

A_G and B_G are constants used to normalize the experimental data. The maximum growth rate, r, and the seed ratio, x_0, of the inoculum size to the maximum carrying capacity were obtained using the logistic population growth model, a subcase of the Richards model well-adapted to bacterial growth [20,21].

$$OD(t) = B_R + \frac{A_R}{\left(1 + \left(\frac{1}{x_0} - 1\right) \cdot \exp\left(-r \cdot t\right)\right)} \qquad (5.2)$$

A_R and B_R are a different set of constants used to normalize the experimental data.

Figure 3 shows the normalized variation of the evolution of the optical density of the 50 µL droplet aliquot at 600 nm and the corresponding fit to the logistic model yielding (x_0 = 0.0077 ± 0.001) and (r = 0.0140 ± 0.0004 s^{-1}). The curve shows a short lag phase (T*lag* = 191 ± 14 min), an exponential growth phase from 200 to 450 min and a stationary phase after 500 min. From the Gompertz-Zwietering (k_Z = 0.0035 ± 0.0004 s^{-1}), the data fits particularly well to both models (solid red line for the logistic growth model) with a residual error ($\chi^2 = 1.67 \cdot 10^{-3}$) for the Gompertz-Zwietering model and ($\chi^2 = 1.60 \cdot 10^{-3}$) for the logistic growth model. We will therefore use this growth curve and its parametrization as a reference throughout the disclosed results.

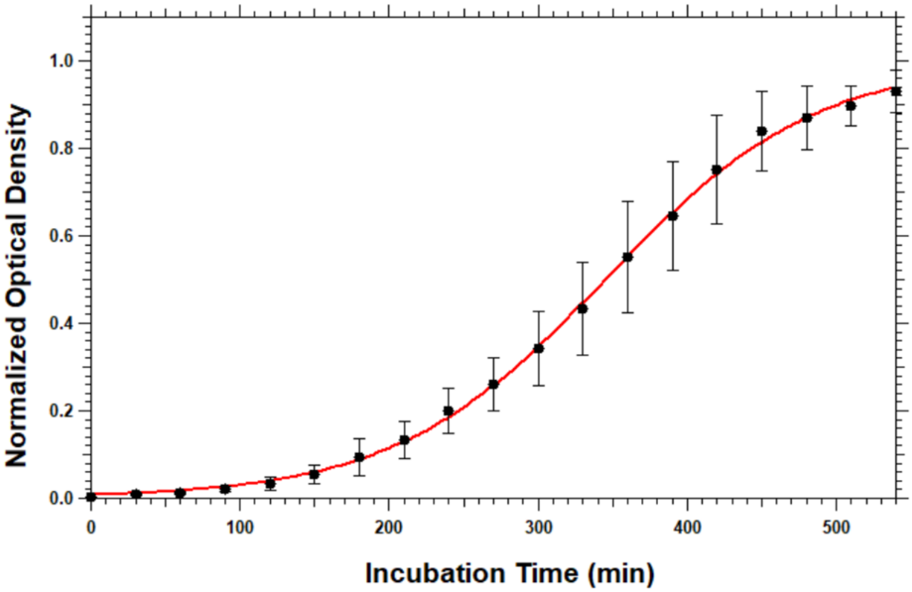

Figure 5.3: Normalized variation of the evolution of the optical density of the 50 µL droplet aliquot at 600 nm and the corresponding fit to the logistic model. This is an average growth curve obtained by measurements over multiple experiments carried out over several weeks growing Escherichia coli in liquid LB.

5.5.2. Reference growth curve using fluorescence microscopy.

Another common way to count bacterial cells to determine growth, in particular for biofilm formation studies [1–3], is to apply particle analysis methods to microscopy images recorded either directly in brightfield, in phase-contrast, or in fluorescence using either bacterial autofluorescence [15] or external dyes. SYBR Green I is a well-known DNA-intercalating dye with an enhanced fluorescence yield when stacked between DNA base pairs [22]. It is by no means a specific marker of bacteria, but we determined it has an irreversible high staining efficiency (> 95%) for bacterial cells with a high signal-to-noise fluorescent signal when excited around 480 nm. In addition, it requires less than 20 minutes to stain a 1 mL sample and the low background signal from unbound SYBR Green molecules allows measurement without additional washing steps. To generate the growth curve, a culture aliquot was taken at set times from the initial seeding of the LB medium, stained with SYBR Green, then deposited on a glass surface and imaged using fluorescence microscopy. Figure 4A shows six of these images, representing the fluorescence image at 0, 60, 116, 171, 235, and 292 minutes of the liquid culture. The images were background-subtracted using a rolling ball method with a radius of 10 pixels in order to remove autofluorescence from the glass slide as well as contributions from unbound dye and cells outside of the focal plane. Visually, there is a clear increase in the number of bacteria present on the surface and the overall fluorescent intensity. The next step consisted of quantifying this evolution. The images generated were, therefore, further processed to perform an accurate count of the number of bacteria present in the microscope field of view (82 x 82 μm) using the particle analysis algorithms from Image J. All images were first thresholded using the same settings to restrict the images acquired to the fluorescence signal with an intensity above 29,000 on the 16-bit scale and, thus, generate a binary image. When a high number of cells are present, it becomes difficult to delimit individual bacteria. We, therefore, used a watershed algorithm [23] to better separate adjacent bacteria cells and thereby improve the accuracy of the particle counting analysis. In order to accurately select bacterial cells and avoid counting other objects such as debris and surface artifacts, the known typical dimensions of *E. coli* [24,25] need to define a minimum acceptable particle area and circularity. Typically, we selected particles above 3μm^2 with circularity values between 0.0 and 0.8. The circularity (c) is a parameter that describes how close an object is to a true circle and is defined by [26].

$$c = 4 \cdot \pi \cdot \frac{A}{p^2} \tag{5.3}$$

where A is the area and p the perimeter. An A value of 1 indicates a perfect circle whereas c draws closer to zero (0) for more elongated polygonal objects.

Figure 4B shows the result of the image processing and the quantification of the recorded frames including those in Figure 3. Each bacterium present in the microscope FOV is counted as a particle, given the restricted values accepted for size and circularity. The reconstructed growth curve shows a very short lag phase, similarly to the one obtained by absorbance measurements (Figure 3) but reaches the stationary phase much earlier and much faster than the reference curve of Figure 3. Compared to Figure 3, the exponential growth phase is much shorter. There are many possible factors contributing to this. First, the surface can have an effect on surface growth. Indeed, attachment to a surface can enhance growth or even promote the assembly of bacteria already grown [27]. However, depositing an aliquot of the culture liquid and imaging it immediately after a short staining period should minimize this effect. Therefore, we believe that the observed shorter exponential growth phase is more likely to be an artifact introduced by the surface, the measurement method and the image processing. Indeed, it is well known that non-fixed cells do not readily adsorb into a solid surface [28], which is a requirement for a surface-oriented method like microscopy. Furthermore, the imaging method is not able to consider bacteria that are out of the focal plane since the fluorescent signal is too weak and too diffused to contribute to the image. These two elements can contribute to a significant underestimation of the number of bacteria present in the culture aliquot compared to the bulk measurement performed in the spectrophotometer. In addition, the particle counting algorithm and the selection parameters we applied are not perfect and can lead to errors in estimating the number of bacteria present, especially at higher concentrations when the number of surface sites available to bacteria decreases and more than a monolayer is formed. The analysis of histograms obtained from each image, as well as the intensity distribution along a radius of 500 pixels from the center of the image and over 180° (radial profile distribution), was not able to provide a growth curve comparable to the expected result from Figure 3. This underlines the severe limitations of microscopy techniques towards the study and quantification of bacterial growth. Our proposed direct measurement method can circumvent some of these limitations.

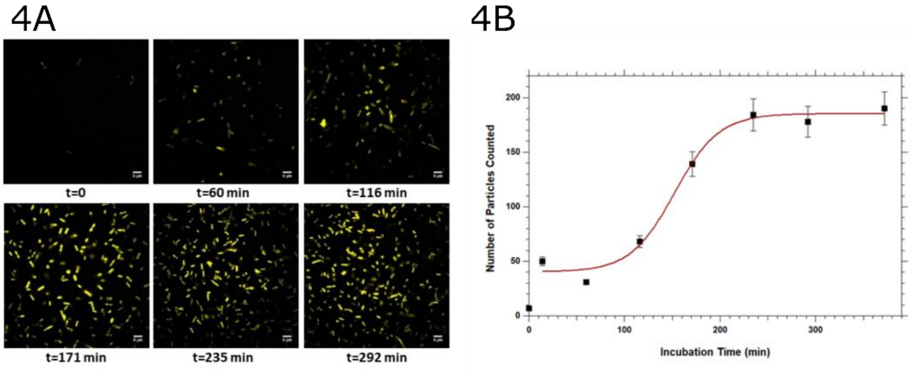

Figure 5.4: 4A, time evolution from microscopy images acquired on a Nikon Ti-U microscope to benchmark our device using SYBR Green stained aliquots of E. coli growing at 37 °C. The intensity scale is identical for all images and the images have been background subtracted using a rolling ball method with a radius of 10 pixels. 4B, growth curve obtained by particle analysis using a watershed algorithm to better separate adjacent cells, then restricting them to a size and circularity according to the expected dimensions of E. coli organisms. The red line is a sigmoid fit that represents the expected curve.

5.5.3. Growth curve using surface cytometer.

Similarly, to the fluorescence microscopy, a culture aliquot was stained with SYBR Green I and deposited onto the sensing surface of the reader. The field of view is much larger than in the microscope, which allows a better averaging of the fluorescent signal from bacteria present in the stained aliquot. In addition, the use of an imaging lens rather than a microscope objective for sample interrogation allows larger depths of fields, and the fluorescence measurement is not constrained to a thin focused volume on the surface, as is the case in microscopy. Therefore, the mean fluorescent signal reported by the system provides a better assessment of the number of bacteria present in the culture aliquot because the permeable SYBR Green dye binds very reliably to DNA material in each bacteria with high efficiency (> 99% of individual bacteria labeled) [30]. This high labeling efficiency allows us to consider that the fluorescence signal averaged over the large field of view of the surface cytometer reader is directly proportional to the number of bacteria present. This indicates that, similarly to the optical density measurement, the available models for bacterial growth apply to our situation. In order to compare optical density with our fluorescence measurements, we will transform the signal collected following equation (5.4).

$$I(t) = \ln\left(\frac{C(t)}{C_0}\right) \tag{5.4}$$

C is the intensity of the signal averaged over the entire CMOS image sensor at incubation time (t) and C_0 is the averaged signal of the CMOS sensor before any sample is introduced. It is the system's baseline, and it is analog to the incident light power used for optical density measurements. I(t) constitutes a direct measurement and does not require complex image post-processing. Figure 5 shows the typical growth curve obtained and the fit to the logistic population growth model [21]. The fit was obtained in two steps in order to avoid biasing the algorithm. First, the low and high asymptotes (A_R and B_R constants in equation (5.2)) were determined by holding the seed ratio, x_0, and the maximum growth rate, r, equal to the values determined for the reference optical density curve (Figure 3) since the aliquots tested came from the same culture sample. Then, once the data was normalized, A_R and B_R were held to 1 and 0, respectively, while the other parameters were adjusted to minimize the residual error (χ2) and determine the apparent values for the growth curve using equation (5.2).

We obtained $x_0 = 0.017 \pm 0.005$ and $r = 0.0120 \pm 0.0009\ s^{-1}$ with $\chi 2 = 4.77 \cdot 10^{-3}$. These values are still in good agreement with the reference parameters obtained in Figure 3. The data in Figure 5 was obtained by averaging the signal over the 3 consecutive measurements of each independent triplicate data point by systematically removing the highest and lowest values. Data points below the known LOD were ignored in the fit and omitted from Figure 5. For comparison purposes, the first reliable data point for the growth curve obtained by the surface cytometer was offset to overlap with the optical density curve. The error bars represent $\pm 2 \cdot \sigma$ where σ is the standard deviation. The fit to the Gompertz-Zwietering model yielded $k_Z = 0.0031 \pm 0.0007\ s^{-1}$ and Tlag = 165 ± 4 min with $\chi 2 = 5.43 \cdot 10^{-4}$. Compared with Figure 3, the Gompertz-Zwietering model fits slightly better with the surface cytometer reader data. This is understandable in this case because the model defines

Tlag to always occur at 6.6% of the upper asymptote, which is more fitting for the surface cytometer data since there is a higher uncertainty on data points just above the LOD. The lag phase is slightly shorter than for the optical density measurement, which is likely due to the lack of sensitivity of the reader for low signals when only a few bacteria are present. The onset of the exponential growth phase and its duration before reaching the stationary phase are, however, well in line with those obtained by absorbance measurements, which gives a good argument towards the relevance of the measurements using our device. The stationary phase plateau is slightly more pronounced than for the absorbance curve, which could originate from signal saturation on the CMOS sensor.

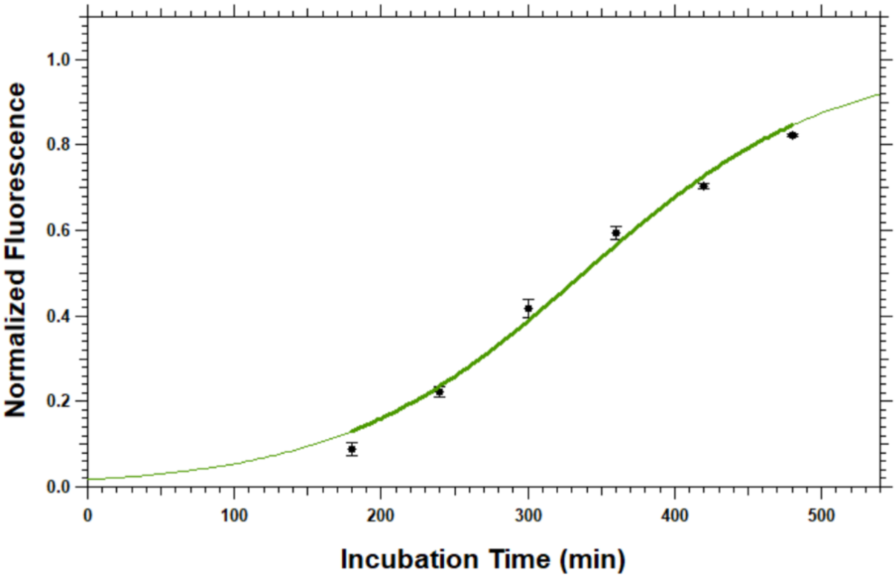

Figure 5.5: The growth curve with normalized intensity obtained through growth monitoring using our surface cytometer with SYBR Green stained samples of E. coli grown at 37 °C in LB.

5.6 Conclusions

In this chapter, we introduced a newly designed surface cytometer for the detection and quantification of bacterial biofilm samples on surfaces. We performed a study of bacterial growth curves and the benchmarking against two routinely used methods for generating bacterial growth curves, so as to validate the capacity of our CMOS-based fluorescence detection system. We have proven our system's usability for accurate and reliable determination of bacterial growth assessment in a culture aliquot using model Gram-negative bacteria (*E. coli*). We have also demonstrated the ability to generate bacterial growth curves that show the same trend as the ones obtained by a gold-standard scattering method. Compared with other imaging techniques, such as fluorescence microscopy, the proposed device has several clear advantages, including a higher field of view and depth of field, which place it in an ideal position to measure bacteria biofilms on surfaces with minimal sample preparation and in only a few minutes. In addition, our measurement method provides a direct result without the need for complex post-processing.

6

Summary and outlook

Recent advancements in optical technologies have shown very promising results in the field of cytometry and its industrial applications. More specifically, innovations in image sensing technologies like CCD and CMOS sensors are making it possible to reduce the overall complexity and cost of the devices. Furthermore, advancements in computational imaging and data processing are allowing us to recover more information from sensed data. All of this comes together to deliver novel devices and methods that allow faster results to be achieved, which is a key factor independently of whether we are using cytometry for clinical applications or environmental monitoring.

This thesis has focused on advancing the field of image cytometry by introducing two novel devices and validating them in key industrial applications. The capacity of this technology has been demonstrated to reach the industry-required levels of detection by quantifying low levels of microorganisms. It has also been shown to minimize the time required to achieve results by bringing tests' duration down to a few minutes as opposed to hours or days with traditional technologies. An effort has also been made to ensure the devices can be portable and easily powered to allow for their in-field use in industrial, ambulatory or outpatient clinical applications.

The concept of Fourier image cytometry was introduced in chapter 2. We discussed its working principles, created a design and implemented an image cytometer capable of enhancing the FOV and DOF (i.e.

maximizing sample volume) while generally maintaining the inexpensive optical and electronic components and simple opto-mechanical contraption. A prototype was built and tested in a laboratory environment to achieve a proof-of-concept demonstration that created the path to take the device to industrial validation.

In chapter 3, the Fourier image cytometer was adapted for industrial use, specifically for the measurement of waterborne microorganisms. Performance was validated with different concentrations of *E. coli*, phytoplankton, *L. pneumophila* and *S. cerevisiae*, which are all microorganisms of high environmental and societal interest. The device implemented achieved a significant combined increase in FOV (>24mm^2) and DOF (≈1 mm) when compared to classical state-of-the-art imaging techniques. The detection limit was proven to be as low as 0.2 cells per ml when an ad-hoc fluidic system was employed to concentrate hundreds of milliliters of sample down to a measurable quantity with a single capture. The ability to apply the Fourier image cytometer to multi-parameter analysis was demonstrated by providing results, which were able to characterize microorganisms by size, complexity, fluorescence emission and concentration. This newly developed device is able to replace high-end cumbersome instrumentation, particularly when fast in-field sample measurements are required. For these experiments an alpha version of the device was used. This alpha version required some further industrialization of the opto-mechanical assembly and optimization of the device optics and processing algorithms to meet some industry requirements.

The optimization of the Fourier image cytometer was the focus of chapter 4, along with its validation in a fully industrial and in-field operation in order to quantify the efficacy of ballast water treatment systems. After introducing some enhancements to our design, a beta prototype of the optical reader was implemented as a field-portable device. After an initial validation in laboratory phytoplankton organisms, the device was taken to an industrial setup for a study of phytoplankton in fresh and marine water environments. This was carried out both before and after processing the water with ballast water treatment systems based on UV radiation and chlorine exposure. We designed a method to measure the microorganism's vitality with our optical device using a modulated excitation light source. The experiment included a comparison with a flow cytometry system, being the current standard in the field, and the results indicate a comparable performance between the two technologies.

Finally, in chapter 5, a novel device was introduced for the purpose of analyzing bacterial presence over surfaces. This is of key interest for point-of-care applications in many clinical, environmental and food processing situations. The device was validated by studying its performance on the measurement of bacterial growth curves. With the objective of enhancing the measurement field and continuing to use generally low-cost components, the surface cytometer was a CMOS-based fluorescence detection system that focused on maximizing the readable surface area of the sample. The device was designed to obtain a FOV of 300 mm^2 with a spatial resolution of 280 μm. While it was not able to resolve individual bacteria with said spatial resolution, the large FOV allowed it to perform an overall quantification of the bacterial biofilm on the surface.

Outlook

The results that have been demonstrated in this thesis show promising prospects for advancement in the field of image cytometry. The two devices introduced, and the results yielded by experimentation and industrial validation, prove that both technologies could be very valuable in their respective fields of application. That said, a few challenges remain in order to achieve the level of performance and the reliance of the systems in industrial setups.

One main challenge is with regard to sample processing. Particularly in the case of the Fourier image cytometer, relying on specific fluorescence labelling protocols was necessary in order to achieve the differentiation between debris and microorganisms when environmental or industrial waters were tested. While the device itself was kept as a low-cost alternative, the use of specific antibodies for labelling increased the cost and complexity of the sample processing. Two options could be pursued in order to improve this in the future. The first one is to focus on the optical device and introduce optics that will allow for a better separation of particles of different sizes over the sensor area, thereby applying an optical filtering to the signal detected and simplifying the post-processing after detection. The challenge with this is that it is likely to increase the costs of the device as more sophisticated elements are introduced into the system. The second one consists in leveraging recent advancements in computational imaging and introduce techniques such as compressive sampling or machine learning algorithms to better characterize the particles within a sample. The challenge here is gathering enough data for each typology of sample for these algorithms to work. Environmental waters and biological samples in general can vary extensively, making it difficult to be able to standardize them on a code level approach.

In the case of the surface cytometer, further validation in a real setting is necessary in order to truly provide evidence of the device's performance. The experiments carried out were in a controlled laboratory environment that did not replicate all of the challenges of in-field measurements. The device would need to be enhanced to a compact and portable industrial prototype. It is expected that through this industrialization process, improvements in the optical system and the processing algorithms will be introduced.

In general, the objective of the wider research and development initiatives of which this thesis took part, was to develop industrially applicable cytometry systems for environmental and biomedical applications. On doing so, the focus was, not only on the development of the systems and in-lab validation of their performance, but also on their industrial validation. This means that starting with a formulated concept and the fundamental technologies to implement, our objective was to bring the systems beyond their initial proof-of-concepts (TRL 3) up to a system demonstration (TRL 7). The complexities brought by the nature of the samples and the aforementioned challenge, are evidence that even though the two systems covered by this thesis are technically and scientifically sound, they still require further development in order to fully meet industry requirements. The continued development on the technology introduced herewith must focus on further exploiting these initial results aiming to create a first commercial system.

Bibliography

[1] H. M. Shapiro, “Pages_from_Practical_Flow_Cytometry.pdf.” .

[2] M. L. Verso, “Some nineteenth century pioneers of haematology,” *Med. Hist.*, vol. 15, no. 1, pp. 55–67, 1971.

[3] W. H. De Vos *et al.*, “Optical microscopy,” *Surf. Charact. A User’s Sourceb.*, vol. 77, no. September, pp. 64–75, 2007, doi: 10.1002/9783527612451.ch1.

[4] “Global Flow Cytometry Market,” 2016.

[5] “2015 Global healthcare outlook,” 2015.

[6] W. H. De Vos, L. Van Neste, B. Dieriks, G. H. Joss, and P. Van Oostveldt, “High content image cytometry in the context of subnuclear organization,” *Cytom. Part A*, vol. 77, no. 1, pp. 64–75, 2010, doi: 10.1002/cyto.a.20807.

[7] S. Ah Lee, X. Ou, J. E. Lee, and C. Yang, “Chip-scale fluorescence microscope based on a silo-filter complementary metal-oxide semiconductor image sensor.,” *Opt. Lett.*, vol. 38, no. 11, pp. 1817–9, 2013.

[8] A. F. Coskun, I. Sencan, T.-W. Su, and A. Ozcan, “Wide-field lensless fluorescent microscopy using a tapered fiber-optic faceplate on a chip.,” *Analyst*, vol. 136, no. 17, pp. 3512–3518, Sep. 2011, doi: 10.1039/c0an00926a.

[9] A. F. Coskun, I. Sencan, T. W. Su, and A. Ozcan, “Lensfree fluorescent on-chip imaging of transgenic Caenorhabditis elegans over an ultra-wide field-of-view,” *PLoS One*, vol. 6, no. 1, p. e15955, Jan. 2011, doi: 10.1371/journal.pone.0015955.

[10] H. Zhu, S. O. Isikman, O. Mudanyali, A. Greenbaum, and A. Ozcan, “Optical imaging techniques for point-of-care diagnostics,” *Lab Chip*, vol. 13, no. 1, pp. 51–67, Jan. 2012, doi: 10.1039/c2lc40864c.

[11] H. Zhu, S. Mavandadi, A. F. Coskun, O. Yaglidere, and A. Ozcan, “Optofluidic fluorescent imaging cytometry on a cell phone,” *Anal. Chem.*, vol. 83, no. 17, pp. 6641–6647, 2011.

[12] D. Tseng *et al.*, “Lensfree microscopy on a cellphone.,” *Lab Chip*, vol. 10,

no. 14, pp. 1787–1792, Jul. 2010, doi: 10.1039/c003477k.

[13] et. al. R. S. Weinstein, “An array microscope for ultrarapid virtual slide processing and telepathology. Design, fabrication and validation study,” *Hum. Pathol.*, vol. 35, no. 11, pp. 1303–1314, 2004.

[14] and M. H. M. Levoy, R. Ng, A. Adams, M. Footer, “Light field microscopy,” *ACM Trans. Graph.*, vol. 25, no. 3, p. 924, 2006.

[15] G. Zheng, R. Horstmeyer, and C. Yang, “Wide-field, high-resolution Fourier ptychographic microscopy,” *Nat. Photonics*, vol. 7, no. 9, pp. 739–745, Jul. 2013, doi: 10.1038/nphoton.2013.187.

[16] A. M. Maiden, M. J. Humphry, F. Zhang, and J. M. Rodenburg, “Superresolution imaging via ptychography,” *J. Opt. Soc. Am. A*, vol. 28, no. 4, p. 604, 2011, doi: 10.1364/JOSAA.28.000604.

[17] T. R. Hillman, T. Gutzler, S. A. Alexandrov, and D. D. Sampson, “reconstruction with synthetic aperture Fourier holographic optical microscopy,” *Opt. Express*, vol. 17, no. 10, pp. 220–230, 2009.

[18] “Waterborne disease could cost over $500 million annually in U.S.,” *Center for Disease Control*, 2010. [Online]. Available: https://www.cdc.gov/media/pressrel/2010/r100714.

[19] M. A. Shannon, P. W. Bohn, M. Elimelech, J. G. Georgiadis, B. J. Marĩas, and A. M. Mayes, “Science and technology for water purification in the coming decades,” *Nature*, vol. 452, no. 7185, pp. 301–310, 2008, doi: 10.1038/nature06599.

[20] A. A. M. Lima *et al.*, “Persistent Diarrhea Signals a Critical Period of Increased Diarrhea Burdens and Nutritional Shortfalls: A Prospective Cohort Study among Children in Northeastern Brazil,” *J. Infect. Dis.*, vol. 181, no. 5, pp. 1643–1651, 2000, doi: 10.1086/315423.

[21] European Centre for Disease Prevention and Control, *Antimicrobial resistance surveillance in Europe 2014*. 2013.

[22] L. P. Rompré A, Servais P, Baudart J, de-Roubin MR, “Detection and enumeration of coliforms in drinking water: current methods and emerging approaches.,” *J. Microbiol. Methods*, vol. 49, pp. 31–54, 2002.

[23] H. Zhu, O. Yaglidere, T.-W. Su, D. Tseng, and A. Ozcan, “Cost-effective and compact wide-field fluorescent imaging on a cell-phone.,” *Lab Chip*, vol. 11, no. 2, pp. 315–322, Jan. 2011, doi: 10.1039/c0lc00358a.

[24] H. C. Koydemir *et al.*, “Rapid imaging, detection and quantification of Giardia lamblia cysts using mobile-phone based fluorescent microscopy and machine learning,” *Lab Chip*, vol. 15, no. 5, pp. 1284–

1293, 2015, doi: 10.1039/c4lc01358a.

[25] H. Zhu, U. Sikora, and A. Ozcan, “Quantum dot enabled detection of Escherichia coli using a cell-phone,” *Analyst*, vol. 137, no. 11, pp. 2541–2544, 2012, doi: 10.1039/c2an35071h.

[26] P. Kozma *et al.*, “A novel handheld fluorescent microarray reader for point-of-care diagnostic,” *Biosens. Bioelectron.*, vol. 47, pp. 415–420, Sep. 2013, doi: 10.1016/j.bios.2013.03.043.

[27] Pandey Govind, “Model Organisms Used in Molecular Biology or Medical Research,” *Int. Res. J. Pharm.*, vol. 2, no. 11, pp. 62–65, 2011.

[28] P. H. Shetty and L. Jespersen, “Saccharomyces cerevisiae and lactic acid bacteria as potential mycotoxin decontaminating agents,” *Trends Food Sci. Technol.*, vol. 17, no. 2, pp. 48–55, 2006, doi: 10.1016/j.tifs.2005.10.004.

[29] C. Venkataraman, L. Y. Gao, S. Bondada, and Y. A. Kwaik, “Identification of putative cytoskeletal protein homologues in the protozoan host Hartmannella vermiformis as substrates for induced tyrosine phosphatase activity upon attachment to the Legionnaires’ disease bacterium, Legionella pneumophila,” *J Exp Med*, vol. 188, no. 3, pp. 505–514, 1998, doi: 10.1084/jem.188.3.505.

[30] D. Claus, D. Iliescu, and P. Bryanston-Cross, “Quantitative space-bandwidth product analysis in digital holography,” *Appl. Opt.*, vol. 50, no. 34, p. H116, 2011, doi: 10.1364/AO.50.00H116.

[31] J. W. Goodman, “Introduction to Fourier Optics McGraw-Hill Series in Electrical and Computer Engineering,” *Quantum Semiclassical Opt. J. Eur. Opt. Soc. Part B*, vol. 8, no. 5, p. 491, 1996.

[32] J. M. Pérez, M. Jofre, P. Martínez, M. A. Yáñez, V. Catalan, and V. Pruneri, “An image cytometer based on angular spatial frequency processing and its validation for rapid detection and quantification of waterborne microorganisms,” *Analyst*, vol. 140, no. 22, pp. 7734–7741, 2015, doi: 10.1039/c5an01338k.

[33] V. Kannan, “Globalization and government regulations: Invasive species management in an era of independece,” *a J. Crit. Writ. Fall*, vol. 10, no. 1, 2015.

[34] J. Moreno-Andrés, L. Romero-Martínez, A. Acevedo-Merino, and E. Nebot, “Determining disinfection efficiency on E. faecalis in saltwater by photolysis of H2O2: Implications for ballast water treatment,” *Chem. Eng. J.*, vol. 283, pp. 1339–1348, 2016, doi: 10.1016/j.cej.2015.08.079.

[35] N. Bax, A. Williamson, M. Aguero, E. Gonzalez, and W. Geeves, “Marine invasive alien species: a threat to global biodiversity,” *Mar. Policy*, vol. 27, no. 4, pp. 313–323, 2003, doi: 10.1016/S0308-597X(03)00041-1.

[36] H. Seebens, M. T. Gastner, and B. Blasius, “The risk of marine bioinvasion caused by global shipping.,” *Ecol. Lett.*, vol. 16, no. 6, pp. 782–90, Jun. 2013, doi: 10.1111/ele.12111.

[37] P. K. Dunstan and N. J. Bax, “Management of an invasive marine species: defining and testing the effectiveness of ballast-water management options using management strategy evaluation,” *ICES J. Mar. Sci.*, vol. 65, no. 6, pp. 841–850, Apr. 2008, doi: 10.1093/icesjms/fsn069.

[38] IMO, “Application of International Convention for the Control and Management of Ships’ Ballast Water and Sediments, 2004,” *IMO Doc. Resolut. A.1088(28)*, no. February, p. London:IMO, 2013, doi: 10.1163/187529988X00184.

[39] R. Rivas-Hermann, J. Köhler, and A. E. Scheepens, “Innovation in product and services in the shipping retrofit industry: a case study of ballast water treatment systems,” *J. Clean. Prod.*, vol. 106, pp. 443–454, 2015, doi: 10.1016/j.jclepro.2014.06.062.

[40] P. P. Stehouwer, A. Buma, and L. Peperzak, “A comparison of six different ballast water treatment systems based on UV radiation, electrochlorination and chlorine dioxide.,” *Environ. Technol.*, vol. 36, no. 13–16, pp. 2094–104, Jan. 2015, doi: 10.1080/09593330.2015.1021858.

[41] L. Maranda, A. M. Cox, R. G. Campbell, and D. C. Smith, “Chlorine dioxide as a treatment for ballast water to control invasive species: Shipboard testing,” *Mar. Pollut. Bull.*, vol. 75, no. 1, pp. 76–89, 2013, doi: 10.1016/j.marpolbul.2013.08.002.

[42] N. Hashemi, J. S. Erickson, J. P. Golden, K. M. Jackson, and F. S. Ligler, “Microflow Cytometer for optical analysis of phytoplankton,” *Biosens. Bioelectron.*, vol. 26, no. 11, pp. 4263–4269, 2011, doi: 10.1016/j.bios.2011.03.042.

[43] S. Sanchez-Ferandin, F. Leroy, F. Y. Bouget, and F. Joux, “A new, sensitive marine microalgal recombinant biosensor using luminescence monitoring for toxicity testing of antifouling biocides,” *Appl. Environ. Microbiol.*, vol. 79, no. 2, pp. 631–638, 2013, doi: 10.1128/AEM.02688-12.

[44] J. Wollschläger, A. Nicolaus, K. H. Wiltshire, and K. Metfies, “Assessment of North Sea phytoplankton via molecular sensing: A method evaluation,” *J. Plankton Res.*, vol. 36, no. 3, pp. 695–708, 2014,

doi: 10.1093/plankt/fbu003.

[45] J. P. Meneely, K. Campbell, C. Greef, M. J. Lochhead, and C. T. Elliott, “Development and validation of an ultrasensitive fluorescence planar waveguide biosensor for the detection of paralytic shellfish toxins in marine algae,” *Biosens. Bioelectron.*, vol. 41, no. 1, pp. 691–697, 2013, doi: 10.1016/j.bios.2012.09.043.

[46] M. J. W. Veldhuis and G. W. Kraay, “Application of flow cytometry in marine phytoplankton research: current applications and future perspectives,” *Sci. Mar.*, vol. 64, no. 2, pp. 121–134, 2000, doi: 10.3989/scimar.2000.64n2121.

[47] U. Schreiber, “Chlorophyll Fluorescence,” *Small Fruits Rev.*, vol. 1, no. 3, pp. 61–67, 2001, doi: 10.1300/J301v01n03_06.

[48] M. J. W. Veldhuis, F. Fuhr, J. P. Boon, and C. C. ten Hallers-Tjabbers, “Treatment of ballast water; how to test a system with a modular concept?,” *Environ. Technol.*, vol. 27, no. 8, pp. 909–921, 2006, doi: 10.1080/09593332708618701.

[49] M. A. O’Connell, B. A. Belanger, and P. D. Haaland, “Calibration and assay development using the four-parameter logistic model,” *Chemom. Intell. Lab. Syst.*, vol. 20, no. 2, pp. 97–114, Sep. 1993, doi: 10.1016/0169-7439(93)80008-6.